A Harmonic-Fourier Spectral Limited-Area Model with an External Wind Lateral Boundary Condition*

QIU-SHI CHEN, LE-SHENG BAI, AND DAVID H. BROMWICH

Polar Meteorology Group, Byrd Polar Research Center, The Ohio State University, Columbus, Ohio

(Manuscript received 27 October 1995, in final form 24 June 1996)

ABSTRACT

In comparison to the Tatsumi's spectral method, the harmonic-Fourier spectral method has two major advantages. 1) The semi-implicit scheme is quite efficient because the solutions of the Poisson and Helmholtz equations are readily derived. 2) The lateral boundary value problem of a limited-area model is easily solved. These advantages are the same as those of the spherical harmonics used in global models if the singularity at the pole points for a globe is considered to be the counterpart of the lateral boundary condition for a limited region.

If a limited-area model is nested in a global model, the prediction of the limited-area model at each time step is the sum of the inner part and the harmonic part predictions. The inner part prediction is solved by the double sine series from the inner part equations for the limited-area model. The harmonic part prediction is derived from the prediction of the global model. An external wind lateral boundary method is proposed based on the basic property of the wind separation in a limited region. The boundary values of a limited-area model in this method are not given at the closed boundary line, but always given by harmonic functions defined throughout the limited domain. The harmonic functions added to the inner parts at each time step represent the effects of the lateral boundary values on the prediction of the limited-area model, and they do not cause any discontinuity near the boundary.

Tests show that predicted motion systems move smoothly in and out through the boundary, where the predicted variables are very smooth without any other boundary treatment. In addition, the boundary method can also be used in the most complicated mountainous region where the boundary intersects high mountains. The tests also show that the adiabatic dynamical part of the limited-area model very accurately predicts the rapid development of a cyclone caused by dry baroclinic instability along the east coast of North America and a lee cyclogenesis case in East Asia. The predicted changes of intensity and location of both cyclones are close to those given by the observations.

1. Introduction

Spectral methods have been used successfully and extensively in global atmospheric models (Bourke 1974; Hoskins and Simmons 1975; Baede et al. 1979; etc.). In comparison to finite-difference methods, spectral methods can give very accurate results with relatively few degrees of freedom. There are almost no computational dispersion and no systematic phase errors in wave advection with spectral methods. Because of the difficulty in choosing appropriate basis functions having the same advantages as the spherical harmonics used in global models, spectral methods have not been frequently used in limited-area models. Some efforts have been made to overcome this difficulty by Tatsumi (1986) and Fulton and Schubert (1987a,b). Modified double Fourier series and a Chebyshev spectral method are used by them, respectively. Recently, a spectral method also has been studied by Haugen and Machenhauer (1993), who use Fourier series with cyclic boundary conditions, and by Juang and Kanamitsu (1994), who use a spectral method similar to that of Tatsumi (1986) to predict deviations from a global model in a regional model.

Tatsumi (1986) introduced two nonorthogonal additional terms into the Fourier series to solve the time-dependent lateral boundary conditions. The sinusoidal-subtracted sine–cosine series are useful for computing the spatial derivatives, but do not have the same convenience for solving the Poisson and Helmholtz equations as the spherical harmonic series used in global models. Based on a comparison between the spherical harmonic series and Tatsumi's (1986) spectral method used in global and limited-area models, respectively, the spherical harmonic series used in global models has two major advantages over Tatsumi's (1986) spectral method. 1) There is no singularity at the pole points in the

*Byrd Polar Research Center Contribution Number 1009.

Corresponding author address: Qiu-shi Chen, Byrd Polar Research Center, The Ohio State University, 1090 Carmack Rd., Columbus, OH 43210.
E-mail: qchen@polarmet1.mps.ohio-state.edu

spectral global model. If the singularity at the pole points of a globe is considered as the counterpart of the lateral boundary condition of a limited region, it means that the lateral boundary conditions for the model are dealt with easily and naturally. 2) In the spectral global model, it is easier to implement the semi-implicit time-integration scheme, which involves very few extra computations at each time step, but generally increases the size of the time step by a factor of 6 compared to that used in the explicit scheme. This is because spherical harmonics are the eigenfunctions of the Laplacian operator and the solutions of the Poisson and Helmholtz equations can be derived easily.

Recently, a spectral method, which is called a harmonic-Fourier (hereafter referred to as H-F), or a harmonic-sine and cosine series expansion proposed by Chen and Kuo (1992a,b) (hereafter referred to as CK92a and CK92b), has been used for the spectral representation of a variable on a rectangular domain. It is proved in CK92a that the computation for the Laplacian operator and the derivation of the solutions for the Poisson and Helmholtz equations are very straightforward using the H-F spectral method. Thus, the semi-implicit scheme will be more efficient in this spectral method than in the modified double Fourier series used by Tatsumi (1986). In addition, the H-F spectral method has another advantage in that the lateral boundary problem can be solved easily and naturally.

Lateral boundaries are an intrinsic feature of a limited-area model. If a limited-area model is nested in a global model with a ''one-way'' influence method during time integration, the boundary values obtained from the global model may be incompatible with the variables within the region predicted by the limited-area model. In principle, there are two approaches to dealing with this lateral boundary value problem.

One is to specify the boundary values in such a manner as to make the problem well posed. For example, Charney (1962) showed that an appropriate set of boundary conditions for the barotropic vorticity equation is to specify the normal velocity everywhere on the boundary and potential vorticity at inflow points. The complication associated with this approach accrues for the unmodified system of the governing equations. Analytic results of Oliger and Sundstrom (1978) indicate that the initial boundary value problem for the hydrostatic primitive equations is ill posed with any specification of pointwise boundary conditions. The essential cause of the ill posedness might be eliminated by applying boundary conditions to each vertical mode independently (Hack and Schubert 1981). An alternate reduced system based on symmetric hyperbolic partial differential equations is found to be well posed (Browning and Kreiss 1986). It should be pointed out that this approach is further complicated by discretization schemes and errors in the boundary data. It seems difficult to solve all the computational boundary problems for a limited-area model by using only this approach.

The second approach is used in the case that the problem with the prescribed boundary values is not well posed. To reduce the amplitude of spurious solutions near the boundary due to ill-posed boundary conditions, it is necessary to employ a lateral boundary treatment that can effectively reduce lateral boundary noise during the integration. These methods include the insertion of a highly diffusive layer contiguous to the boundary (Benwell et al. 1971), a divergence control method (Okamura 1975), a method of modification of the tendencies at the boundary (Kesel and Winninghoff 1972; Perkey and Kreitzberg 1976), the boundary relaxation method (Davies 1976), etc. In the limited-area spectral models of Tatsumi (1986) and Juang and Kanamitsu (1994), the boundary relaxation method is used to reduce the lateral boundary noise.

In this paper, besides testing the harmonic-sine spectral method, we will present a new method for specifying the lateral boundary values of limited-area models. This method is also used in the case that the problem with the prescribed boundary values is not well posed.

From a global perspective, a limited region R defined for a limited-area model is only a part of the global surface. The other part of the global surface outside the region R is referred to as the external region Q. From the global perspective, the wind field in the limited region R depends not only upon the vorticity and divergence within the region R, but also on those of the external region Q.

Based on the studies of CK92a and Chen et al. (1996), the wind field in a limited area can be separated into two parts. One is the internal wind that depends only upon the vorticity and divergence within the region R. No matter how the vorticity and divergence vary in the external region, the internal wind does not vary. The other part is the external wind that depends only on the vorticity and divergence outside the region R. No matter how the vorticity and divergence vary within the region R, the external wind does not change. This is the basic property of the above wind separation in a limited region.

If a limited-area model is formulated in terms of the vorticity and divergence equations (instead of the momentum equations) and is nested in a global model by the one-way method, based on the basic property of wind separation shown above, only the internal wind in the limited area can be predicted from the vorticity and divergence equations of the limited-area model; the external wind in the limited area must be derived from the prediction of the global model. The total wind in the limited region at each time step is the sum of the internal and external winds predicted by the two models, respectively. That the external wind is added to the internal wind at each time step represents the effect of the lateral boundary values predicted by the global model on the wind prediction of the limited-area model. This is the basic idea for solving the lateral boundary problem of a limited-area model.

In addition to the wind field, a similar idea can also

be used to solve the lateral boundary values for scalar variables, such as geopotential height, temperature, and surface pressure. Based on CK92a and CK92b, a scalar variable is separated into harmonic and inner parts. The two separations for a scalar variable and wind vector are different. The harmonic and inner parts are used to express the separation of scalar variables, such as the streamfunction, velocity potential, and geopotential height, etc., but the external and internal winds are utilized to denote the separation of the wind vector (Chen et al. 1996).

Because the boundary value of a variable for the harmonic-sine series expansion is simpler than that of the harmonic-cosine one, only the harmonic-sine series expansion is used in this paper. The equations for scalar variables of the limited-area model are all transformed into the equations of their inner parts, whose boundary values are homogeneous. Thus, the inner part equations of the limited-area model can easily be solved by the double sine series.

The harmonic parts of the scalar variables in the limited region are derived from the prediction of the global model. The total prediction of these scalar variables in the limited region at each time step is the sum of the inner and harmonic parts. This is a simple method to prescribe the lateral boundary values of scalar variables.

The external wind and the harmonic parts of scalar variables are all the harmonic functions. In this boundary method, the lateral boundary value of a variable is not just given at a closed line of the boundary, but it is always given by a harmonic function defined in the whole limited domain. Because the derivatives of a harmonic function up to second order are continuous, the harmonic function must be very smooth in the region up to the boundary. The harmonic function added to the inner part cannot cause any discontinuity near the boundary. Thus, the new boundary method is quite different from some other artificial pragmatic techniques (Benwell et al. 1971; Okamura 1975; Davies 1976) mentioned above, and it has a relatively strong theoretical basis, especially for the wind field. Tests of this boundary method will show that the predicted motion near the boundary is smooth without any other boundary treatment.

It should be noted that the primary appeal of a spectral method is its high accuracy. Finite-difference discretizations give algebraic convergence, while a properly formulated spectral method gives exponential convergence. Recently, Kuo and Williams (1992) used a simple example in one-dimensional space to study the accuracy of regional spectral methods and found that Tatsumi's (1986) spectral method does not possess exponential convergence. In this paper, we do not explore the exponential convergence of the H-F spectral method, but we want to show that the semi-implicit time integration scheme and the external wind lateral boundary method are much more efficiently and conveniently implemented by the H-F spectral method than by Tatsumi's spectral method.

The paper is organized as follows. The governing model equations formulated in terms of the vorticity and divergence equations are shown in section 2. The vertical finite-difference representation of the model equations is discussed in the appendix. The equations for the streamfunction, velocity potential, and generalized geopotential are presented in section 3. All of the model equations are transformed into their inner parts in this section. The solution of the equations in the vertical mode space and their semi-implicit time integration scheme are discussed in section 4. Section 5 outlines the external wind lateral boundary method for a limited-area model. The basic idea of how the one-way and two-way interactive procedures for a limited-area model nested in a global model are implemented based on the external wind boundary method is discussed in this section. Tests of predictions of the explosive development of a cyclone over the east coast of North America and a lee-cyclogenesis case in East Asia computed by the H-F spectral limited-area model with the external wind lateral boundary method are discussed in section 6.

2. The basic equations

The vertical coordinate σ is defined by

$$\sigma = \frac{p}{p_*}, \tag{2.1}$$

where $p_*(x, y, t)$ is the surface pressure. The symbols are defined as usual.

The momentum equation is

$$\frac{\partial \mathbf{V}}{\partial t} = -(f + \zeta)\mathbf{k} \times \mathbf{V} - \dot{\sigma}\frac{\partial \mathbf{V}}{\partial \sigma} - \nabla\left(\phi + \frac{1}{2}\mathbf{V}\cdot\mathbf{V}\right) - RT\nabla \ln p_* + P_{\mathbf{V}} + K_{\mathbf{V}}. \tag{2.2}$$

The thermodynamic equation is

$$\frac{\partial T}{\partial t} = -\mathbf{V}\cdot\nabla T - \dot{\sigma}\frac{\partial T}{\partial \sigma} + \frac{RT}{C_p P}\omega + P_T + K_T. \tag{2.3}$$

The continuity equation is

$$\frac{\partial \ln p_*}{\partial t} = -\mathbf{V}\cdot\nabla \ln p_* - \nabla\cdot\mathbf{V} - \frac{\partial \dot{\sigma}}{\partial \sigma}. \tag{2.4}$$

The continuity equation of water vapor is

$$\frac{\partial q}{\partial t} = -\mathbf{V}\cdot\nabla q - \dot{\sigma}\frac{\partial q}{\partial \sigma} + P_q + K_q. \tag{2.5}$$

The hydrostatic equation is

$$\frac{\partial \phi}{\partial \sigma} = -\frac{RT}{\sigma}. \tag{2.6}$$

It is assumed that

$$f = f_0 + f' \tag{2.7}$$

$$T = T_0(\sigma) + T' = T_0(\sigma) + [T(x, y, \sigma, t) - T_0(\sigma)], \tag{2.8}$$

where f_0 is the averaged value of Coriolis parameter in the integration region and f' is its deviation. Equation (2.8) means that the temperature field is divided into a basic state portion, $T_0(\sigma)$, that depends only on sigma and is statically stable, and a deviation from the basic state, T'.

The terms P_U, P_V, P_T, and P_q can be written as

$$P_U = -\frac{m}{p_*}\frac{\partial}{\partial\sigma}J_u \tag{2.9}$$

$$P_V = -\frac{m}{p_*}\frac{\partial}{\partial\sigma}J_v \tag{2.10}$$

$$P_T = \frac{1}{C_p}\left\{Q_R + Q_L + Q_D - \frac{g}{p_*}\left[\frac{\partial}{\partial\sigma}J_s - C_{pd}T(d-1)\frac{\partial}{\partial\sigma}J_q\right]\right\} \tag{2.11}$$

$$P_q = S_q - \frac{g}{p_*}\frac{\partial}{\partial\sigma}J_q. \tag{2.12}$$

In (2.9)–(2.12), J_u, J_v, J_s, and J_q represent net parameterized vertical fluxes of momentum, dry static energy ($C_pT + \phi$), and moisture, and they include fluxes due to convection and boundary layer turbulence. Here, m is the map scale factor, and Q_R, Q_L, and Q_D represent heating due, respectively, to radiation, internal phase changes (including evaporation of precipitation), and the internal dissipation of kinetic energy associated with the P_U and P_V terms. Here, S_q denotes the rate of change of q due to precipitation.

The terms K_u, K_v, K_T, and K_q represent the influence of unsolved horizontal scales. Their treatment differs from that of P_U, P_V, P_T, and P_q terms in that it does not involve a physical model of subgrid-scale processes, but rather a numerically convenient form of scale selective diffusion of a magnitude determined empirically to ensure realistic behavior of resolved scales.

a. The vorticity and divergence equations

The vorticity and divergence equation are derived from (2.2) and written in the form

$$\frac{\partial\zeta}{\partial t} = -f_0\delta + m^2\Omega_{\text{adv}} + m^2K_\zeta \tag{2.13}$$

$$\frac{\partial\delta}{\partial t} = f_0\zeta - m^2\nabla^2(\phi + RT_0\ln p_*) + m^2D_{\text{adv}} - m^2\nabla^2E + m^2K_\delta, \tag{2.14}$$

where

$$\zeta = \mathbf{k}\cdot\nabla\times\mathbf{V} = m^2\left[\frac{\partial}{\partial x}\left(\frac{v}{m}\right) - \frac{\partial}{\partial y}\left(\frac{u}{m}\right)\right] \tag{2.15}$$

$$\delta = \nabla\cdot\mathbf{V} = m^2\left[\frac{\partial}{\partial x}\left(\frac{u}{m}\right) + \frac{\partial}{\partial y}\left(\frac{v}{m}\right)\right] \tag{2.16}$$

$$\Omega_{\text{adv}} = -\left[\frac{u}{m}\frac{\partial(f'+\zeta)}{\partial x} + \frac{v}{m}\frac{\partial(f'+\zeta)}{\partial y}\right] - (f'+\zeta)\frac{\partial}{m^2} + \frac{\partial F_v}{\partial x} - \frac{\partial F_u}{\partial y} \tag{2.17}$$

$$D_{\text{adv}} = \frac{v}{m}\frac{\partial(f'+\zeta)}{\partial x} - \frac{u}{m}\frac{\partial(f'+\zeta)}{\partial y} + (f'+\zeta)\frac{\zeta}{m^2} + \frac{\partial F_u}{\partial x} + \frac{\partial F_v}{\partial y} \tag{2.18}$$

$$E = \frac{u^2+v^2}{2} \tag{2.19}$$

and

$$F_u = -\dot\sigma\frac{\partial}{\partial\sigma}\left(\frac{u}{m}\right) - RT'\frac{\partial\ln p_*}{\partial x} + \frac{P_U}{m} \tag{2.20}$$

$$F_v = \dot\sigma\frac{\partial}{\partial\sigma}\left(\frac{v}{m}\right) - RT'\frac{\partial\ln p_*}{\partial y} + \frac{P_V}{m}. \tag{2.21}$$

The main parts of Ω_{adv} and D_{adv} are the horizontal and vertical advection, so that Ω_{adv} and D_{adv} are referred to as the vorticity and divergence advection terms, respectively. The terms K_ζ and K_δ are derived from K_u and K_v, and they represent the influence of unsolved horizontal scales on vorticity and divergence, respectively.

b. The vertical finite-difference form of the equations

Let U, V, Ω, and D be

$$U = \frac{u}{m}, \qquad V = \frac{v}{m},$$

$$\Omega = \frac{\zeta}{m^2} \qquad D = \frac{\delta}{m^2}. \tag{2.22}$$

It is assumed that

$$m^2 = m_0^2 + (m^2)', \tag{2.23}$$

where m_0^2 is the averaged value of m^2 over the integration region and $(m^2)'$ is its deviation. The vertical distribution of variables is shown in Fig. 1. Based on the vertical difference form derived in the appendix, the continuity equation (A.5) can be rewritten as

$$\frac{\partial\ln p_*}{\partial t} + m_0^2\,\mathbf{\Pi}\,\mathbf{D} = P_{\text{adv}}, \tag{2.24}$$

where

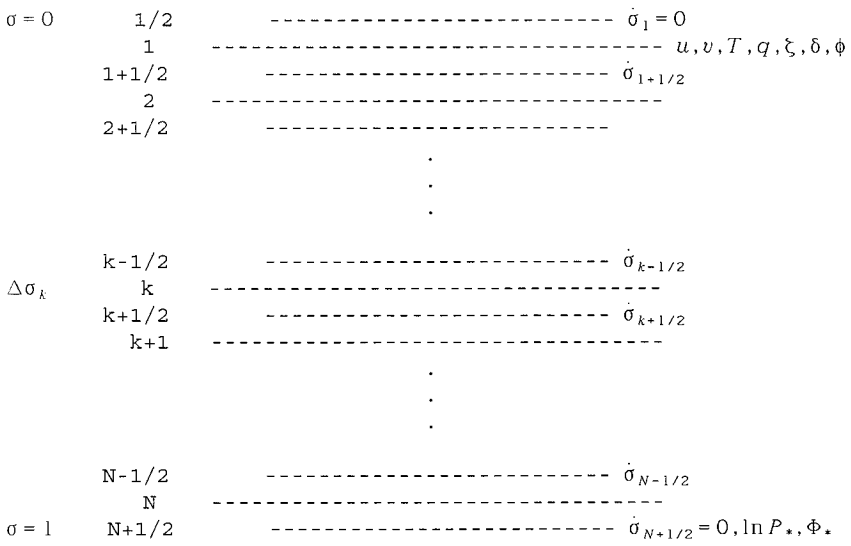

FIG. 1. The vertical distribution of the variables.

$$\mathbf{D} = \begin{bmatrix} D_1 \\ D_2 \\ \cdot \\ \cdot \\ D_n \end{bmatrix},$$

$$\mathbf{\Pi} = (\Delta\sigma_1, \ldots, \Delta\sigma_k, \ldots, \Delta\sigma_N). \quad (2.25)$$

If the basic equations are written in column-vector form, (A.40) and (A.43) become

$$\frac{\partial \mathbf{\Omega}}{\partial t} + f_0 \mathbf{D} = \Omega_{\text{adv}} + \mathbf{K}_\zeta \quad (2.26)$$

and

$$\frac{\partial \mathbf{D}}{\partial t} - f_0 \mathbf{\Omega} + \nabla^2(\boldsymbol{\phi} + R\mathbf{T}_0 \ln P_*) = \mathbf{D}_{\text{adv}} - \nabla^2 \mathbf{E} + \mathbf{K}_\delta. \quad (2.27)$$

The thermodynamic equation (A.33) is rewritten as

$$\frac{\partial \mathbf{T}}{\partial t} + m_0^2 \mathbf{F}\mathbf{D} = \mathbf{T}_{\text{adv}} + \mathbf{P}_T + \mathbf{K}_T, \quad (2.28)$$

where $\mathbf{T}_{\text{adv}}$ becomes

$$\mathbf{T}_{\text{adv}} = \mathbf{T}_{\text{hor}} + \mathbf{T}_{\text{ver}} + \mathbf{T}_{\text{spa}} - (m^2)' \mathbf{F}\mathbf{D}. \quad (2.29)$$

The hydrostatic equation (A.28) is

$$\boldsymbol{\phi} = \boldsymbol{\phi}_* + R\mathbf{B}\mathbf{T}. \quad (2.30)$$

Substituting it into (2.27), we have

$$\frac{\partial \mathbf{D}}{\partial t} - f_0 \mathbf{\Omega} + \nabla^2(\boldsymbol{\phi}_* + R\mathbf{B}\mathbf{T}_v + R\mathbf{T}_0 \ln P_*) = \mathbf{D}_{\text{adv}} - \nabla^2 \mathbf{E} + \mathbf{K}_\delta. \quad (2.31)$$

The equation for the mixing ratio (A.45) is

$$\frac{\partial \mathbf{q}}{\partial t} = \mathbf{Q}_{\text{adv}} + \mathbf{P}_q + \mathbf{K}_q. \quad (2.32)$$

The equations (2.24), (2.26), (2.28), (2.31), and (2.32) are the basic equations for the variables $\ln p_*$, Ω, T, D, and q.

3. The inner part equations of the model

a. The separation of the scalar variables and wind

The limited-area model is defined in a closed region R shown by Fig. 2a. The region shown by Fig. 2b is

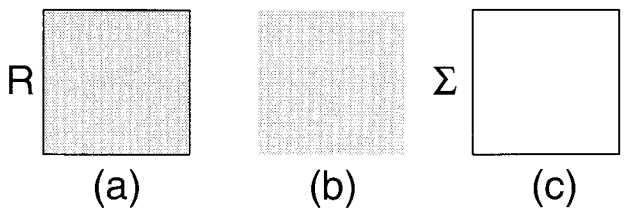

FIG. 2. (a) The closed region R, (b) the open region R without boundary, and (c) the boundary of the region R.

an open region without the boundary, and it is also referred to as interior of R or within the region R. The closed line Σ shown by Fig. 2c is the boundary of region R. Based on the harmonic-sine series expansion (CK92a), a scalar variable A, such as temperature or geopotential height, defined on closed R can be divided into the harmonic and inner parts, $A = A_i + A_h$, where the harmonic part A_h satisfies the Laplace equation and Dirichlet boundary condition

$$\begin{cases} \nabla^2 A_h = 0, & \text{in interior of R,} \\ A_h\big|_\Sigma = A(\Sigma), & \text{at the boundary } \Sigma, \end{cases} \tag{3.1}$$

and the inner part A_i is determined by $A_i = A - A_h$. The inner part A_i vanishes at the boundary Σ automatically and can be expanded in a double sine series. The streamfunction and velocity potential on closed R are separated by

$$\psi = \psi_h + \psi_i, \qquad \chi = \chi_h + \chi_i, \tag{3.2}$$

where the inner parts ψ_i and χ_i satisfy the Poisson equations

$$\begin{cases} \nabla^2\psi_i = \Omega, \quad \nabla^2\chi_i = D, & \text{in interior of R,} \\ \psi_i\big|_\Sigma = 0, \quad \chi_i\big|_\Sigma = 0, & \text{at the boundary } \Sigma, \end{cases} \tag{3.3}$$

and they are easily solved by the double sine series. The internal wind on closed R is defined by

$$U_I = -\frac{\partial\psi_i}{\partial y} + \frac{\partial\chi_i}{\partial x}, \qquad V_I = \frac{\partial\psi_i}{\partial x} + \frac{\partial\chi_i}{\partial y}, \tag{3.4}$$

and the external wind on closed R is derived by

$$U_E = U - U_I, \qquad V_E = V - V_I. \tag{3.5}$$

The harmonic parts, ψ_h and χ_h, fulfill the Laplace equations

$$\nabla^2\,\psi_h = 0, \qquad \nabla^2\,\chi_h = 0 \tag{3.6}$$

in the interior of R, and at the boundary Σ they satisfy

$$\left(-\frac{\partial\psi_h}{\partial y} + \frac{\partial\chi_h}{\partial x}\right)\bigg|_\Sigma = U_E\big|_\Sigma,$$

$$\left(\frac{\partial\psi_h}{\partial x} + \frac{\partial\chi_h}{\partial y}\right)\bigg|_\Sigma = V_E\big|_\Sigma. \tag{3.7}$$

The separation of wind field into the internal and external winds based on (3.4) and (3.5) is different from that of scalar variables.

Because the inner parts are expressed by the double sine series, $\nabla^2\psi_i$ and $\nabla^2\chi_i$ at the boundary Σ become

$$\nabla^2\psi_i\big|_\Sigma = 0, \qquad \nabla^2\chi_i\big|_\Sigma = 0. \tag{3.8}$$

If the vorticity and divergence need to be computed on closed R from the inner parts, they can be derived by

$$\nabla^2\psi_i + \Omega\big|_\Sigma = \Omega, \qquad \nabla^2\chi_i + D\big|_\Sigma = D, \tag{3.9}$$

where the symbol $\Omega\big|_\Sigma$ is defined on closed R and denoted by

$$\Omega\big|_\Sigma = \begin{cases} \Omega, & \text{at the boundary } \Sigma, \\ 0, & \text{in interior of R.} \end{cases} \tag{3.10}$$

To avoid discontinuity of (3.9) at the boundary, the following method can be used. The vorticity and divergence are separated into their harmonic and inner parts expressed by

$$\Omega = \Omega_i + \Omega_h, \qquad D = D_i + D_h, \tag{3.11}$$

where Ω_h and D_h satisfy Laplace equations $\nabla^2\Omega_h = 0$ and $\nabla^2 D_h = 0$ with the Dirichlet boundary values $\Omega_h\big|_\Sigma = \Omega\big|_\Sigma$ and $D_h\big|_\Sigma = D\big|_\Sigma$, respectively. Introducing two new variables, $\psi_{h,i}$ and $\chi_{h,i}$, they are a portion of the inner parts of streamfunction and velocity potential, respectively, and they satisfy the Poisson equations

$$\nabla^2\psi_{h,i} = \Omega_h, \qquad \nabla^2\chi_{h,i} = D_h, \tag{3.12}$$

with zero Dirichlet boundary value. Based on (3.11), the inner parts Ω_i and D_i can be derived by $\Omega_i = \nabla^2\psi_i - \nabla^2\psi_{h,i}$ and $D_i = \nabla^2\chi_i - \nabla^2{}_{h,i}$. Thus, the vorticity and divergence on closed R computed from the inner parts are expressed by

$$\nabla^2(\psi_i - \psi_{h,i}) + \Omega_h = \Omega, \qquad \nabla^2(\chi_i - \chi_{h,i}) + D_h = D. \tag{3.13}$$

If an equation $A = B$ is satisfied on closed R, then by applying the harmonic-sine spectral method (3.1) to both sides and based on the uniqueness of the harmonic function for the Dirichlet boundary value, it follows that the following equations

$$A_h = B_h \quad \text{and} \quad A_i = B_i \tag{3.14}$$

are satisfied on closed R.

b. *The governing equations of the inner parts of the streamfunction and velocity potential*

Let us introduce two variables $\psi_{\text{adv},i}$ and $\chi_{\text{adv},i}$, which satisfy the following equations:

$$\nabla^2\psi_{\text{adv},i} = \Omega_{\text{adv}}, \qquad \nabla^2\chi_{\text{adv},i} = D_{\text{adv}}, \tag{3.15}$$

with the homogeneous Dirichlet boundary values. The variables $\psi_{\text{adv},i}$ and $\chi_{\text{adv},i}$ are referred to as advection variation rates of the inner parts of the streamfunction and velocity potential, respectively.

To simplify notations, let F denote a finite Fourier sine transform operator in the two-dimensional space, that is,

$$F[f_I(x, y)] = F_{I,mn} = \frac{4}{L_x L_y}\int_0^{L_x}\int_0^{L_y} f_I(x, y)\sin\frac{m\pi x}{L_x}\sin\frac{n\pi y}{L_y}\,dx\,dy. \tag{3.16}$$

The double Fourier sine series of f_I are

$$f_I(x, y) = F^{-1}[F_{I,mn}] = \sum_{m=1}^{M}\sum_{n=1}^{N} F_I(m, n)\sin\frac{m\pi x}{L_x}\sin\frac{n\pi y}{L_y}, \quad (3.17)$$

where F^{-1} is the inverse Fourier sine transform operator from wave to physical space.

Thus, the solutions of (3.15) are

$$\psi_{\text{adv},i} = -F^{-1}\left[\Omega_{\text{adv},mn}\left(\frac{1}{L_{mn}^2}\right)^{-1}\right] \quad (3.18)$$

and

$$\chi_{\text{adv},i} = -F^{-1}\left[D_{\text{adv},mn}\left(\frac{1}{L_{mn}^2}\right)^{-1}\right], \quad (3.19)$$

where

$$\Omega_{\text{adv},mn} = F[\Omega_{\text{adv}}], \qquad D_{\text{adv},mn} = F[D_{\text{adv}}], \quad (3.20)$$

and L_{mn} is referred to as a horizontal scale of the wave and expressed by

$$\frac{1}{L_{mn}^2} = \frac{m^2\pi^2}{L_x^2} + \frac{n^2\pi^2}{L_y^2}. \quad (3.21)$$

Utilizing (3.18) and (3.19), (2.26) and (2.27) can be solved with zero Dirichlet boundary values, and their solutions are

$$\frac{\partial \boldsymbol{\psi}_i}{\partial t} + f_0\boldsymbol{\chi}_i = \boldsymbol{\psi}_{\text{adv},i} \quad (3.22)$$

$$\frac{\partial \boldsymbol{\chi}_i}{\partial t} + (\boldsymbol{\phi} + R\mathbf{T}_0 \ln p_*)_i - f_0\boldsymbol{\psi}_i = \boldsymbol{\chi}_{\text{adv},i} - \mathbf{E}_i. \quad (3.23)$$

Because the terms K_ζ, K_δ, K_T, and K_q represent the influence of unsolved horizontal scales, their treatment involves a horizontal diffusion solved by the spectral method based on the splitting procedure. The method for solving these terms is described in section 4e, and thus, these terms are temporarily omitted from (3.22) and (3.23).

c. The equation of the inner part of the generalized geopotential height on the constant σ surface

Now we introduce a variable

$$\boldsymbol{\phi}' = \boldsymbol{\Phi} + R\mathbf{T}_0 \ln p_*, \quad (3.24)$$

where $\boldsymbol{\phi}'$ is referred to as the generalized geopotential height in σ coordinates. Because the geopotential height on the constant σ surface depends on the temperature through the hydrostatic equation (2.30), the generalized geopotential height is expressed by

$$\boldsymbol{\phi}' = \boldsymbol{\phi}_* + R\mathbf{B}\boldsymbol{T} + R\boldsymbol{T}_0 \ln p_*. \quad (3.25)$$

Taking the partial derivative with respect to t, (3.25) becomes

$$\frac{\partial \boldsymbol{\phi}'}{\partial t} = R\mathbf{B}\frac{\partial \mathbf{T}}{\partial t} + R\mathbf{T}_0\frac{\partial \ln p_*}{\partial t}. \quad (3.26)$$

Substituting (2.24) and (2.28) into (3.26), the equation of the generalized geopotential becomes

$$\frac{\partial \boldsymbol{\phi}'}{\partial t} + m_0^2\mathbf{AD} = \boldsymbol{\Phi}'_{\text{had}}, \quad (3.27)$$

where matrix $\mathbf{A}$ is

$$\mathbf{A} = R(\mathbf{BF} + \mathbf{T}_0\boldsymbol{\Pi}). \quad (3.28)$$

Here,

$$\boldsymbol{\Phi}'_{\text{had}} \downarrow = R\mathbf{B}\mathbf{T}_{\text{adv}} + R\mathbf{T}_0 P_{\text{adv}} + R\mathbf{B}\mathbf{P}_T \quad (3.29)$$

denotes the variation of the generalized geopotential height caused by the advection and diabatic heating.

Based on (3.14), (3.27) can be rewritten into two equations as

$$\frac{\partial \boldsymbol{\phi}'_i}{\partial t} + m_0^2\mathbf{AD}_i = \boldsymbol{\Phi}'_{\text{had},i}, \quad (3.30)$$

and

$$\frac{\partial \boldsymbol{\phi}'_h}{\partial t} + m_0^2\mathbf{AD}_h = \boldsymbol{\Phi}'_{\text{had},h}. \quad (3.31)$$

Based on (3.10), (3.11), and (3.12), (3.30) is rewritten in the form

$$\frac{\partial \boldsymbol{\phi}'_i}{\partial t} + m_0^2\mathbf{A}\nabla^2\boldsymbol{\chi}_i = \boldsymbol{\Phi}'_{\text{had},i} + m_0^2\mathbf{AD}'_h, \quad (3.32)$$

where

$$\mathbf{D}'_h = \mathbf{D}_h - \mathbf{D}_h\big|_\Sigma = \nabla^2\boldsymbol{\chi}_{h,i} \quad (3.33)$$

is the harmonic part of the divergence in the closed region with zero boundary value. Equations (3.22), (3.23), and (3.32) are the basic equations of the inner parts of the three variables: the streamfunction, velocity potential, and generalized geopotential.

d. The equation of the generalized ageostrophic geopotential

If the inner parts of the streamfunction and geopotential in p coordinates are denoted by $\psi_{p,i}$ and $\phi_{p,i}$, the ageostrophic deviation in the atmospheric motion can be expressed by $\phi_{p,ia} = \phi_{p,i} - f_0\psi_{p,i}$, where $\phi_{p,ia}$ is referred to as an inner part of the ageostrophic geopotential on isobaric surface. In σ coordinates, the generalized ageostrophic geopotential at σ surface is approximately defined by

$$\phi'_{ia} = \phi'_i - f_0\psi_i = (\phi + RT_0 \ln p_*)_i - f_0\psi_i. \quad (3.34)$$

From (3.22) and (3.32), the equation of the generalized ageostrophic geopotential is

$$\frac{\partial \boldsymbol{\phi}'_{ia}}{\partial t} + m_0^2\mathbf{A}\nabla^2\boldsymbol{\chi}_i - f_0^2\boldsymbol{\chi}_i = \boldsymbol{\Phi}'_{\text{had},ia} + m_0^2\mathbf{AD}'_h, \quad (3.35)$$

where

$$\boldsymbol{\Phi}'_{\text{had},ia} = \boldsymbol{\Phi}'_{\text{had},i} - f_0\boldsymbol{\psi}_{\text{adv},i} \quad (3.36)$$

is referred to as the variation of the generalized ageostrophic geopotential caused by advection and diabatic heating.

The velocity potential equation (3.23) can be rewritten as

$$\frac{\partial \boldsymbol{\chi}_i}{\partial t} + \boldsymbol{\phi}'_{ia} = \boldsymbol{\chi}_{\mathrm{adv},i} - \mathbf{E}_i. \tag{3.37}$$

The basic variables for describing the atmospheric motion now become the inner parts of the streamfunction, velocity potential, and generalized ageostrophic geopotential.

4. The inner part equations of the vertical modes and their semi-implicit time-integration scheme

a. The inner part equations of the vertical modes

Equation (3.32) or (3.35) can be transformed into the equation of its vertical mode. We introduce a matrix $\mathbf{E}$ in order that the following relation is satisfied:

$$\mathbf{E}^{-1}\mathbf{A}\mathbf{E} = \mathbf{G} = \mathrm{diag}(gh_1, gh_2, \ldots, gh_N). \tag{4.1}$$

For this purpose, the eigenvectors of the matrix $\mathbf{A}$ are derived and expressed by $\mathbf{E}_j$, $j = 1, \ldots, N$. In (4.1), the matrix $\mathbf{E}$ represents the eigenvector matrix with each column representing an eigenvector $\mathbf{E}_j$. The matrix $\mathbf{E}^{-1}$ is the inverse of the matrix $\mathbf{E}$. The matrix $\mathbf{G}$ is a diagonal matrix with the diagonal elements given by the N eigenvalues, $(gh_1, gh_2, \ldots, gh_N)$, of the matrix $\mathbf{A}$. The values $h_1, h_2, \ldots,$ and h_N are the equivalent depth of the vertical modes.

Let the vertical mode of the variables be

$$\boldsymbol{\chi}_{i^*} = \mathbf{E}^{-1}\boldsymbol{\chi}_i, \quad \boldsymbol{\psi}_{i^*} = \mathbf{E}^{-1}\boldsymbol{\psi}_i, \quad \boldsymbol{\phi}'_{ia^*} = \mathbf{E}^{-1}\boldsymbol{\phi}'_{ia}, \tag{4.2}$$

and thus, the variables in physical space are

$$\boldsymbol{\chi}_i = \mathbf{E}\boldsymbol{\chi}_{i^*}, \quad \boldsymbol{\psi}_i = \mathbf{E}\boldsymbol{\psi}_{i^*}, \quad \boldsymbol{\phi}'_{ia} = \mathbf{E}\boldsymbol{\phi}'_{ia^*}. \tag{4.3}$$

Equations (3.22), (3.37), and (3.35) are multiplied from left by the matrix $\mathbf{E}^{-1}$; then

$$\frac{\partial \boldsymbol{\psi}_{i^*}}{\partial t} + f_0\boldsymbol{\chi}_{i^*} = \boldsymbol{\psi}_{\mathrm{adv},i^*} \tag{4.4}$$

$$\frac{\partial \boldsymbol{\chi}_{i^*}}{\partial t} + \boldsymbol{\phi}'_{ia^*} = \boldsymbol{\chi}_{\mathrm{adv},i^*} - \mathbf{E}_{i^*} \tag{4.5}$$

$$\frac{\partial \boldsymbol{\phi}'_{ia^*}}{\partial t} + m_0^2\mathbf{G}\nabla^2\boldsymbol{\chi}_{i^*} - f_0^2\boldsymbol{\chi}_{i^*} = \boldsymbol{\Phi}'_{\mathrm{had},ia^*} + m_0^2\mathbf{G}\mathbf{D}'_{h^*}, \tag{4.6}$$

where

$$\boldsymbol{\chi}_{\mathrm{adv},i^*} = \mathbf{E}^{-1}\boldsymbol{\chi}_{\mathrm{adv},i}, \qquad \boldsymbol{\psi}_{\mathrm{adv},I^*} = \mathbf{E}^{-1}\boldsymbol{\psi}_{\mathrm{adv},i},$$
$$\boldsymbol{\Phi}'_{had,ia^*} = \mathbf{E}^{-1}\boldsymbol{\Phi}'_{\mathrm{had},ia}, \qquad \mathbf{D}'_{h^*} = \mathbf{E}^{-1}\mathbf{D}'_h. \tag{4.7}$$

The equations (4.4)–(4.6) can be rewritten as

$$\frac{\partial \psi_{i^*k}}{\partial t} + f_0\chi_{i^*k} = \psi_{\mathrm{adv},i^*k}, \tag{4.8}$$

$$\frac{\partial \chi_{i^*k}}{\partial t} + \phi'_{ia^*k} = \chi_{\mathrm{adv},i^*k} - E_{i^*k} \tag{4.9}$$

$$\frac{\partial \phi'_{ia^*k}}{\partial t} + C_k^2\left(\nabla^2 - \frac{1}{L_{0k}^2}\right)\chi_{i^*k} = \Phi'_{\mathrm{had},ia^*k} - C_k^2 D'_{h^*k} \tag{4.10}$$

$$k = 1, 2, \ldots, N \tag{4.11}$$

for each of the vertical modes separately, where C_k is the gravity wave phase speed for the kth vertical mode, and L_{0k} is the radius of deformation of the kth mode, and they are expressed by

$$C_k = m_0(gh_k)^{1/2}, \qquad L_{0k}^2 = \frac{m_0^2 gh_k}{f_0^2} = \left(\frac{C_k}{f_0}\right)^2, \tag{4.12}$$

respectively. The equations for the vertical mode k have the same form as the shallow water equations with equivalent depth, h_k.

b. The solution of the gravity–inertia wave equation in the semi-implicit time-integration scheme

Now introducing a leapfrog scheme,

$$\delta_t X = \frac{X^{t+\Delta t} - X^{t-\Delta t}}{2\Delta t}, \tag{4.13}$$

to analogize the time derivative of a variable X, and using an implicit treatment of the linear gravity wave terms in (4.8)–(4.10), we obtain the following set of prognostic equations:

$$\delta_t\psi_{i^*k} + f_0\overline{\chi}^t_{i^*k} = \psi^t_{\mathrm{adv},i^*k} \tag{4.14}$$

$$\delta_t\chi_{i^*k} + \overline{\phi'_{i^*k}}^{\,t} = \chi^t_{\mathrm{adv},i^*k} - E^t_{i^*k} \tag{4.15}$$

$$\delta_t\phi'_{ia^*k} + C_k^2\nabla^2\overline{\chi}^t_{i^*k} - f_0^2\overline{\chi}^t_{i^*k} = \Phi'^{\,t}_{\mathrm{had},ia^*k} + C_k^2 D'^{\,t}_{h^*k}, \tag{4.16}$$

where

$$\overline{X}^t = \frac{X^{t+\Delta t} + X^{t-\Delta t}}{2}. \tag{4.17}$$

From (4.17), (4.13) becomes

$$\delta_t X = \frac{\overline{X}^t - X^{t-\Delta t}}{\Delta t}. \tag{4.18}$$

Thus, (4.14)–(4.16) can be rewritten as

$$\overline{\psi_{i^*k}}^{\,t} + f_0\Delta t\overline{\chi}^t_{i^*k} = \psi^t_{\mathrm{adv},i^*k}\Delta t + \psi^{t-\Delta t}_{i^*k} \tag{4.19}$$

$$\overline{\chi_{i^*k}}^{\,t} + (\Delta t)\overline{\phi'_{ia^*k}}^{\,t} = (\chi^t_{\mathrm{adv},i^*k} - E^t_{i^*k})\Delta t + \chi^{t-\Delta t}_{i^*k} \tag{4.20}$$

$$\overline{\phi'_{ia^*k}}^{\,t} + C_k^2\Delta t\nabla^2\overline{\chi_{i^*k}}^{\,t} - f_0^2\Delta t\overline{\chi_{i^*k}} = \Delta t\Phi'^{\,t}_{\mathrm{had},ia^*k} + C_k^2\Delta t D'^{\,t}_{h^*k} + \phi'^{\,t-\Delta t}_{ia^*k}. \tag{4.21}$$

Eliminating $\overline{\phi'_{ia^*k}}^{\,t}$ from (4.20) and (4.21), we obtain

$$\nabla^2\overline{\chi_{i^*k}}^t - \left[\frac{1}{(C_k\Delta t)^2} + \frac{1}{L_{0k}^2}\right]\overline{\chi_{i^*k}}^t = F^t_{*k}, \quad (4.22)$$

where the forcing term, F^t_{*k}, is expressed by

$$F^t_{*k} = -\frac{1}{(C_k\Delta t)^2}[-(\Delta t)^2\Phi'^t_{\text{had},ia^*k} - C_k^2(\Delta t)^2 D'^t_{h^*k} - (\Delta t)\phi'^{t-\Delta t}_{ia^*k} + (\chi^t_{\text{adv},i^*k} - E^t_{i^*k})\Delta t + \chi^{t-\Delta t}_{i^*k}]. \quad (4.23)$$

Equation (4.22) is the semi-implicit time integration scheme of the gravity–inertia wave equation, and it describes the averaged velocity potential between two time steps in vertical mode space.

Because the lateral boundary value of the inner part of the velocity potential is homogeneous, the solution of the Helmholtz equation (4.22) can be derived from the double sine series. Based on (3.16) and (3.17), the solution is written in the form

$$\bar{\chi}^t_{i^*k,mn} = -F[F^t_{*k}(x, y)]\left(\frac{1}{L_{mn}^2} + a^2\right)^{-1}, \quad (4.24)$$

where

$$a_k^2 = \frac{1}{(C_k\Delta t)^2} + \frac{1}{L_{0k}^2}. \quad (4.25)$$

After the vertical mode of the velocity potential is obtained from (4.24), the streamfunction can be computed from (4.19) by

$$\bar{\psi}^t_{i^*k} = \psi^t_{\text{adv},i^*k}(\Delta t) + \psi^{t-\Delta t}_{i^*k} - (f_0\Delta t)\bar{\chi}^t_{i^*k}. \quad (4.26)$$

After $\overline{\boldsymbol{\psi}_{i^*}}^t$ is derived, we have

$$\overline{\chi_i}^t = \mathbf{E}\overline{\chi_{i^*}}^t, \qquad \overline{\psi_i}^t = \mathbf{E}\overline{\psi_{i^*}}^t. \quad (4.27)$$

From (4.17) and (4.18), the inner parts of the variables in the next time step are

$$\chi^{t+\Delta t}_{ik} = 2\bar{\chi}^t_{ik} - \chi^{t-\Delta t}_{ik},$$
$$\psi^{t+\Delta t}_{ik} = 2\bar{\psi}^t_{ik} - \psi^{t-\Delta t}_{ik}. \quad (4.28)$$

c. The semi-implicit scheme for surface pressure, temperature, and mixing ratio

After introducing a leapfrog finite difference for the time derivatives and an implicit treatment of the linear gravity wave terms, (2.24), (2.28), and (2.32) can be written as

$$\overline{\ln p}^t + m_0^2\Delta t\boldsymbol{\Pi}\bar{\mathbf{D}}^t = P^t_{\text{adv}}\Delta t + \ln p^{t-\Delta t}_* \quad (4.29)$$

$$\bar{\mathbf{T}}^t + m_0^2\Delta t\mathbf{F}\bar{\mathbf{D}}^t = \mathbf{T}^t_{\text{adv}}\Delta t + \Delta t\mathbf{P}^t_T + \mathbf{T}^{t-\Delta t} \quad (4.30)$$

$$\bar{q}^t = (\mathbf{Q}^t_{\text{adv}} + \mathbf{P}^t_q)\Delta t + \mathbf{q}^{t-\Delta t}. \quad (4.31)$$

Based on (3.14), (4.29)–(4.31) can be separated into two parts. The equations for the inner parts are

$$\overline{\ln p_{*,i}}^t = -m_0^2\Delta t\boldsymbol{\Pi}\overline{D_i}^t + P^t_{\text{adv},i}\Delta t + \ln p^{t-\Delta t}_{*,i} \quad (4.32)$$

$$\overline{\mathbf{T}_i}^t = -m_0^2\Delta t\mathbf{F}\overline{\mathbf{D}_i}^t + \mathbf{T}^t_{\text{adv},i}\Delta t + \Delta t\mathbf{P}^t_{T,i} + \mathbf{T}^{t-\Delta t}_i \quad (4.33)$$

$$\overline{\mathbf{q}_i}^t = (\mathbf{Q}^t_{\text{adv}} + \mathbf{P}^t_q)_i\Delta t + \mathbf{q}^{t-\Delta t}_i \quad (4.34)$$

and the equations for the harmonic parts are

$$\overline{\ln p_{*,h}}^t = -m_0^2\Delta t\Pi\overline{D_h}^t + P^t_{\text{adv},h}\Delta t + \ln p^{t-\Delta t}_{*,h} \quad (4.35)$$

$$\overline{T_h}^t = -m_0^2\Delta t\mathbf{F}\overline{\mathbf{D}_h}^t + \mathbf{T}^t_{\text{adv},h}\Delta t + \Delta t\mathbf{P}^t_{T,h} + \mathbf{T}^{t-\Delta t}_h \quad (4.36)$$

$$\overline{\mathbf{q}_h}^t = (\mathbf{Q}^t_{\text{adv}} + \mathbf{P}^t_q)_h\Delta t + \mathbf{q}^{t-\Delta t}_h, \quad (4.37)$$

where $\overline{\mathbf{D}_i}^t$ in (4.32) and (4.33) can be calculated from (3.13) by

$$\overline{\mathbf{D}_i}^t = \bar{\mathbf{D}}^t - \overline{\mathbf{D}_h}^t = \nabla^2(\overline{\boldsymbol{\chi}_i}^t - \overline{\boldsymbol{\chi}_{h,i}}^t) \quad (4.38)$$

and $\overline{\mathbf{D}_h^t}$ is obtained by the prediction of the global model. The values for the step $t + \Delta t$ can be deduced by

$$X^{t+\Delta t} = 2\overline{X^t} - X^{t-\Delta t}. \quad (4.39)$$

d. The computation of the initial time step

For the initial time steps, we perform three initial steps: a forward step of $\Delta t/4$ and a centered one of $\Delta t/2$, then a centered one of Δt. After these three initial time steps, the basic time scheme with $2\Delta t$ is started. This method is an effective way of reducing the initial shock, especially when using the large time steps permitted by use of the semi-implicit method.

The first forward time step is

$$\delta_t X = \frac{X^{\Delta t/4} - X^{(0)}}{\Delta t/4} \quad (4.40)$$

$$\bar{X}^{\Delta t/8} = \frac{X^{\Delta t/4} + X^{(0)}}{2}. \quad (4.41)$$

Thus,

$$X^{\Delta t/4} = 2\bar{X}^{\Delta t/8} - X^{(0)}. \quad (4.42)$$

The second and third steps are

$$X^{\Delta t/2} = 2\bar{X}^{\Delta t/4} - X^{(0)}, \qquad X^{\Delta t} = 2\bar{X}^{\Delta t/2} - X^{(0)}. \quad (4.43)$$

Then the basic time step is started at $t = \Delta t$.

e. Horizontal diffusion

''Horizontal'' smoothing of streamfunction, velocity potential, and specific humidity is represented by a simple linear fourth-order diffusion applied along the σ coordinate surface:

$$(K_X)_i = -K\nabla^4 X_i, \quad (4.44)$$

where $X_i = \psi_i$, χ_i, or q_i. It is applied in spectral space

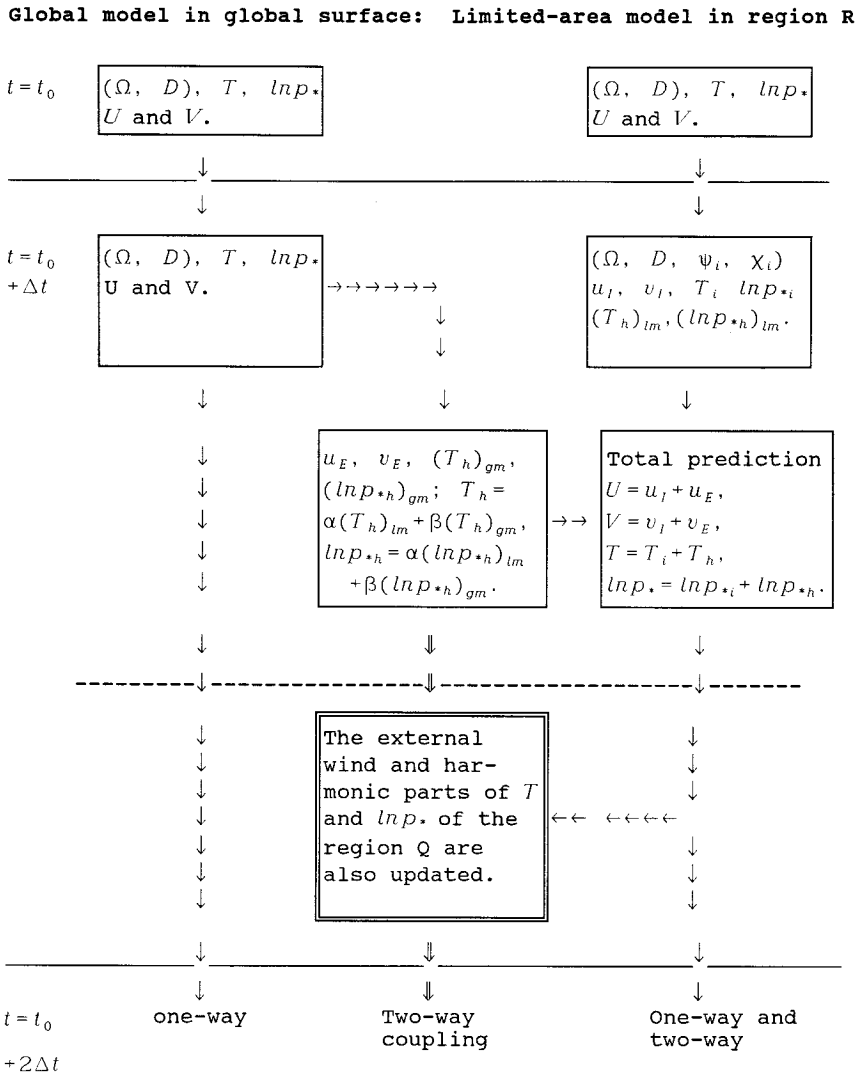

FIG. 3. Outline of the one-way and two-way coupling external wind lateral boundary method between global and limited-area models. (The global surface is the sum of the regions R and Q.)

to $t + \Delta t$ values such that if $(x_i)_n^m$ is a spectral coefficient of X_i computed for time step $t + \Delta t$ prior to diffusion, then the diffused value $\overline{x_i}_n^m$ is given by an implicit scheme as

$$\overline{x_{i_n}}^m = (x_i)_n^m - 2K\Delta t\left(\frac{1}{L_{mn}^2}\right)^2 \overline{x_{i_n}}^m \tag{4.45}$$

or

$$\overline{x_{i_n}}^m = (x_i)_n^m\left[1 + 2K\Delta t\left(\frac{1}{L_{mn}^2}\right)^2\right]^{-1}, \tag{4.46}$$

where L_{mn} is determined by (3.21). A modified diffusion is used for temperature to avoid an unrealistic warming of mountain tops. A computationally convenient form that approximates diffusion on pressure surfaces is used. Equation (4.46) becomes

$$\overline{T_{i_n}}^m = (T_{ic})_n^m + [(T_i)_n^m - (T_{ic})_n^m]\left[1 + 2K\Delta t\left(\frac{1}{L_{mn}^2}\right)^2\right]^{-1}, \tag{4.47}$$

where

$$T_{ic} = \left(p_* \frac{\partial p}{\partial p_*}\frac{\partial T}{\partial p}\right)_{\text{ref}} \ln p_{*_i} \tag{4.48}$$

and $(p_*\partial p/\partial p_*\ \partial T/\partial p)_{\text{ref}}$ denotes reference values, and it varies only with the model level based on the standard ICAO atmosphere.

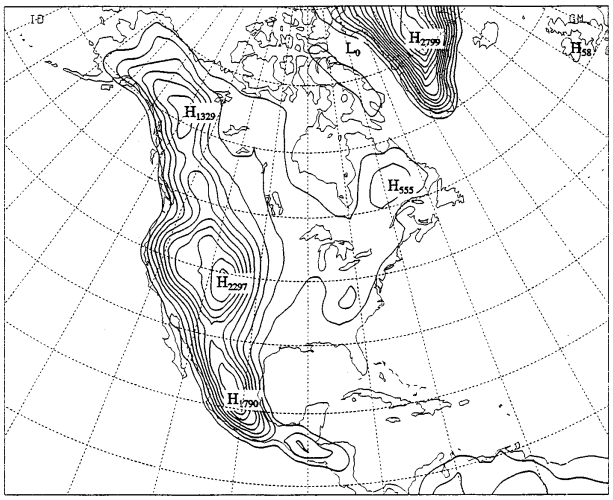

FIG. 4. The topography of model domain centered over North America. Contour interval is 200 m.

5. An external wind lateral boundary method

a. The wind reconstruction and its lateral boundary condition

The basic property of the wind separation into the internal and external winds discussed by CK92a and Chen et al. (1996) will be utilized to solve the lateral boundary problem of a limited-area model. As pointed out in section 1, if a limited-area model is nested in a global model, only the internal wind in the limited area can be predicted from the vorticity and divergence equations of the limited-area model, while the external wind in the limited area must be derived from prediction of the global model.

Based on the equations in section 4, the inner parts, $\psi_i^{t+\Delta t}$ and $\chi_i^{t+\Delta t}$, are predicted by the limited-area model as shown in the right column of Fig. 3. The internal wind is computed by

$$U_I^{t+\Delta t} = -\frac{\partial \psi_i^{t+\Delta t}}{\partial y} + \frac{\partial \chi_i^{t+\Delta t}}{\partial x},$$
$$V_I^{t+\Delta t} = \frac{\partial \psi_i^{t+\Delta t}}{\partial x} + \frac{\partial \chi_i^{t+\Delta t}}{\partial y}. \tag{5.1}$$

The external wind, U_E and V_E, on closed R can be obtained by the natural method (Chen et al. 1996) from the predicted wind (or vorticity and divergence) of the global model as shown in the middle column of Fig. 3. In this natural method, the internal wind on closed R is also derived based on the global model prediction, then the external wind is computed by (3.5). The external wind derived by the natural method satisfies the consistency condition (Chen et al. 1996) automatically.

To compute the advection terms at the time step $t + \Delta t$, it is necessary to know $U^{t+\Delta t}$, $V^{t+\Delta t}$, $\Omega^{t+\Delta t}$, and $D^{t+\Delta t}$ on closed R. The total wind on closed R at each time step is the sum of the internal and external winds expressed by

$$U^{t+\Delta t} = U^{t+\Delta t}{}_E + U^{t+\Delta t}{}_I,$$
$$V^{t+\Delta t} = V^{t+\Delta t}{}_E + V^{t+\Delta t}{}_I. \tag{5.2}$$

Based on (3.9), the vorticity and divergence, $\Omega^{t+\Delta t}$ and $D^{t+\Delta t}$, on closed R are calculated from $\psi_i^{t+\Delta t}$ and $\chi_i^{t+\Delta t}$ by

$$\Omega^{t+\Delta t} = \nabla^2 \psi^{t+\Delta t}{}_i + \Omega|_\Sigma^{t+\Delta t},$$
$$D^{t+\Delta t} = \nabla^2 \chi^{t+\Delta t}{}_i + D|_\Sigma^{t+\Delta t}, \tag{5.3}$$

where $\Omega|_\Sigma^{t+\Delta t}$ and $D|_\Sigma^{t+\Delta t}$ can be obtained from the global model prediction. For avoiding discontinuity of (5.3) at the boundary, based on (3.13), (5.3) can be replaced by

$$\Omega^{t+\Delta t} = \nabla^2(\psi_i^{t+\Delta t} - \psi_{h,i}^{t+\Delta t}) + \Omega_h^{t+\Delta t},$$
$$D^{t+\Delta t} = \nabla^2(\chi_i^{t+\Delta t} - \chi_{h,i}^{t+\Delta t}) + D_h^{t+\Delta t}. \tag{5.4}$$

By this boundary method, the predicted total wind at the boundary of the limited region is not equal to the predicted wind of the global model. Because the vorticity and divergence within the region have been changed by the limited-area model prediction, the wind at the boundary should also change for consistency.

b. The lateral boundary condition for the variables ln p_*, *T, and q*

The harmonic parts of the surface pressure, temperature, and mixing ratio, $\ln p_{*,h}^{t+\Delta t}$, $T_h^{t+\Delta t}$, and $q_h^{t+\Delta t}$, are different from the external wind because they can be predicted not only from the global model but also from the limited-area model by (4.35)–(4.37). The harmonic parts computed from the global model are denoted by $(\ln p_{*,h})_{gm}^{t+\Delta t}$, $(T_h)_{gm}^{t+\Delta t}$, and $(q_h)_{gm}^{t+\Delta t}$, while those calculated from the limited-area model based on (4.35)–(4.37) are expressed by $(\ln p_{*,h})_{lm}^{t+\Delta t}$, $(T_h)_{lm}^{t+\Delta t}$, and $(q_h)_{lm}^{t+\Delta t}$. In general, the harmonic parts derived from the limited-area model have higher resolution (or shorter horizontal scales) than those derived from the global model, especially when higher resolution topography is used in the limited region.

The harmonic part of a scalar variable used as the boundary value of a limited-area model is referred to as a boundary harmonic part. There are two methods to determine the boundary harmonic parts. One method is that the boundary harmonic parts are the same as the harmonic parts derived from the global model, and thus,

$$\ln p_{*,h}^{t+\Delta t} = (\ln p_{*,h})_{gm}^{t+\Delta t},$$
$$T_h^{t+\Delta t} = (T_h)_{gm}^{t+\Delta t}, \qquad q_h^{t+\Delta t} = (q_h)_{gm}^{t+\Delta t}. \tag{5.5}$$

This method is referred to as a simple method.

The other method is called a weighted mean method. In this method, the boundary harmonic parts are weighted mean values of two harmonic parts derived from both the global and limited-area models, and they are expressed by

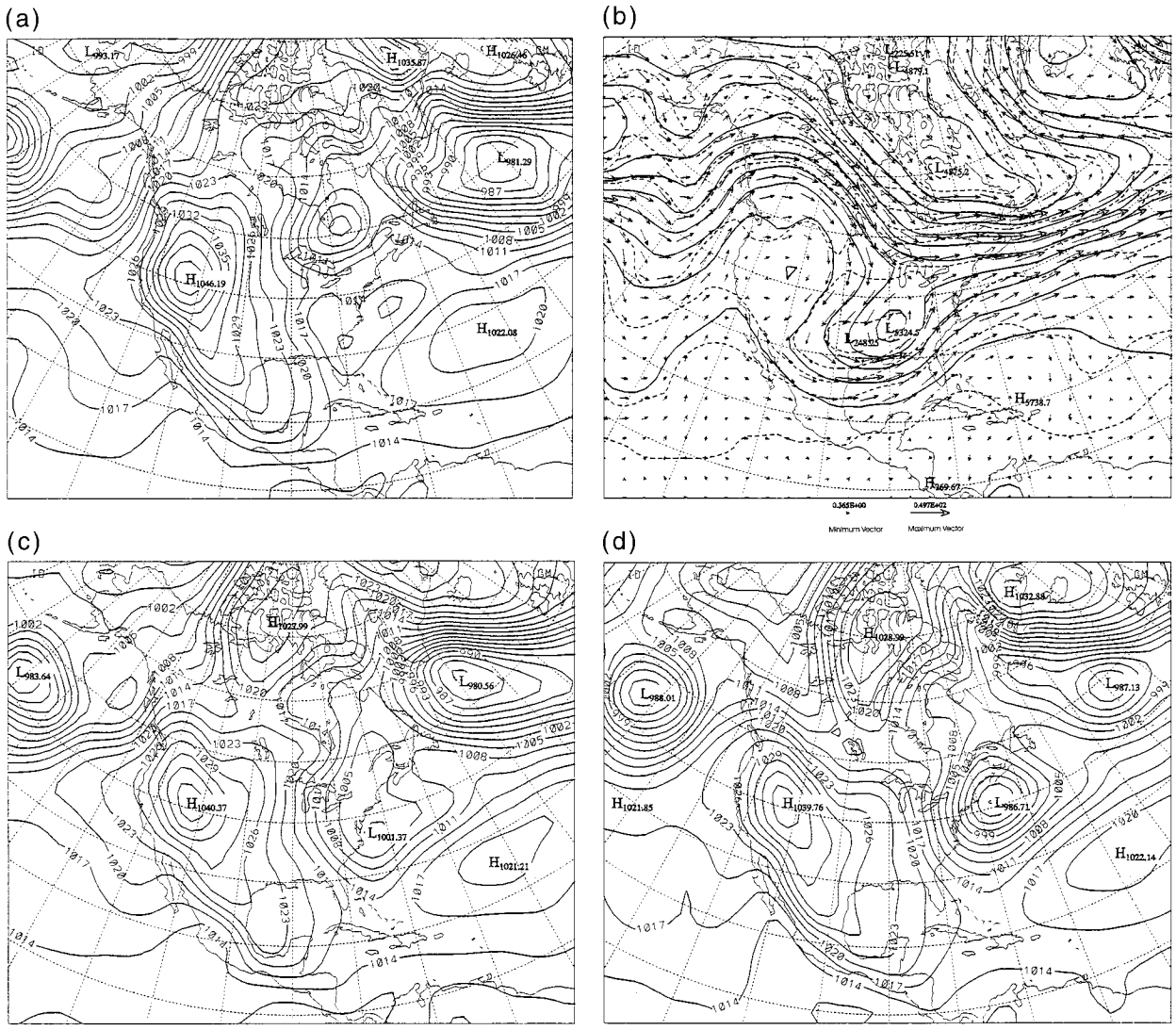

FIG. 5. Observed charts: (a) SLP (3-hPa isobar spacing) at 1200 UTC 4 January 1985; (b) the geopotential height (solid contours at 40-gpm spacing), wind (arrows with scale in meters per second at bottom), and temperature (dashed in 2-K increments) at the 500-hPa level for the same time as in (a); (c) SLP at 0000 UTC 5 January 1985; (d) SLP at 1200 UTC 5 January 1985; (e) SLP at 0000 UTC 6 January 1985; and (f) the geopotential height, wind, and temperature at the 500-hPa level for same time as in (d).

$$\ln p_{*,h}^{t+\Delta t} = \alpha(\ln p_{*,h})_{lm}^{t+\Delta t} + \beta(\ln p_{*,h})_{gm}^{t+\Delta t},$$
$$T_h^{t+\Delta t} = \alpha(T_h)_{lm}^{t+\Delta t} + \beta(T_h)_{gm}^{t+\Delta t},$$
$$q_h^{t+\Delta t} = \alpha(q_h)_{lm}^{t+\Delta t} + \beta(q_h)_{gm}^{t+\Delta t}, \quad (5.6)$$

where $\alpha + \beta = 1$. The simple method is a special case of the weighted mean method when $\alpha = 0$ and $\beta = 1$ in (5.6).

The predicted variables, T, $\ln p_*$, and q at $t + \Delta t$ in the limited region, are the sum of the inner and boundary harmonic parts expressed by

$$\ln p_*^{t+\Delta t} = \ln p_{*,i}^{t+\Delta t} + \ln p_{*,h}^{t+\Delta t},$$
$$T^{t+\Delta t} = T_i^{t+\Delta t} + T_h^{t+\Delta t},$$
$$q^{t+\Delta t} = q_i^{t+\Delta t} + q_h^{t+\Delta t}. \quad (5.7)$$

The method shown by (5.2), (5.3), and (5.7) is referred to as the external wind lateral boundary method, and its goal is to guarantee two properties of the predicted variables at the boundary for the limited-area model: one is consistency or continuity at the boundary, and the other is accuracy.

The inner parts are predicted by the limited-area model in the form of the double sine series. The boundary effects from the global model are represented by the harmonic parts added to the inner parts. The harmonic parts are all harmonic functions, and so are their linear combinations shown by (5.6). The components of the external wind are also harmonic functions. The harmonic functions are very smooth in the closed region up to the boundary, and thus, the sum shown by (5.2) and (5.7) cannot cause any discontinuity near the bound-

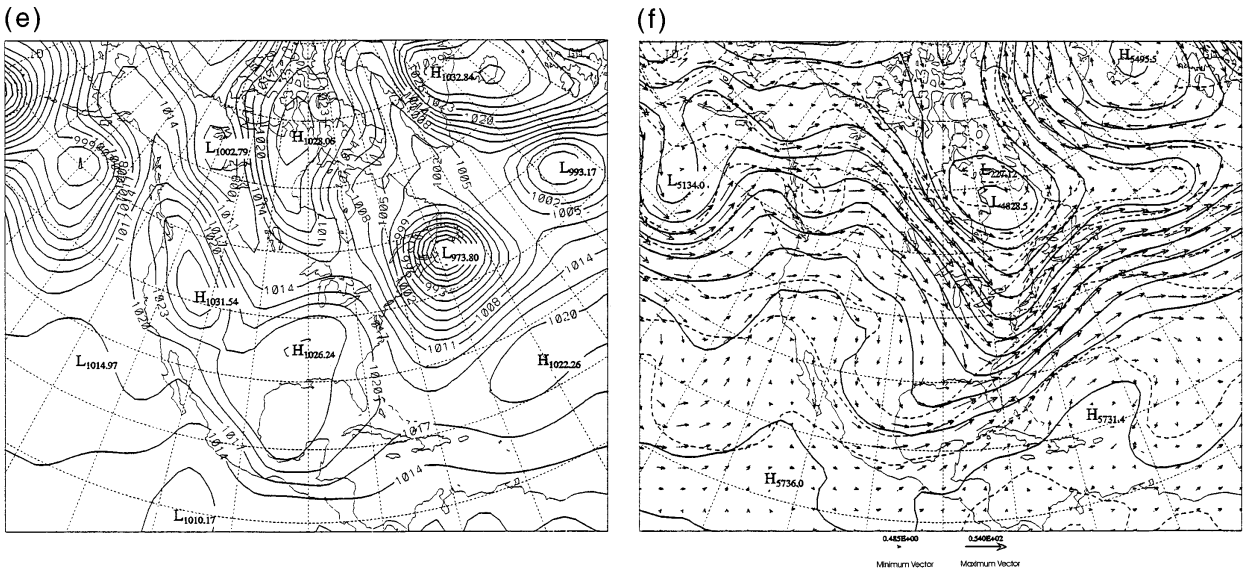

FIG. 5. (*Continued*)

ary. The accuracy of the prediction of the limited-area model depends upon the accuracy of the provided boundary values. The weighted mean method given by (5.6) is designed with a view to obtain more accurate boundary values for the limited-area model than by the simple method.

The main purpose of this paper is to show the property of the consistency or continuity for the external wind lateral boundary method, and thus, only the tests of the simple method are discussed in the next section.

c. The basic idea of a two-way coupling between limited-area and global models

If the feedback from the limited-area model to the global model is needed, the basic idea of a two-way coupling method is also shown in Fig. 3. In the two-way coupling method, the global surface is divided into two parts as shown in section 1: one is the limited area R and the other is the region Q outside the area R. The boundary line between the regions R and Q is denoted by Σ. During two-way coupling, the wind predicted by the limited-area model will be used to update the wind predicted by the global model in the limited area R including the boundary Σ. From the global perspective, the external wind of the region R is related to the vorticity and divergence in the region Q, and inversely, the external wind of the region Q is also related to the vorticity and divergence in the region R. After the vorticity, divergence and wind are updated in the region R, the external wind of the region Q should also be updated in order to obtain the continuous wind at the global surface. The external wind of the region Q can be derived from the updated wind at Σ. A similar method can also be used to treat the variables $\ln p_*$, T, and q.

In this two-way coupling, changes are not only for the wind and the scalar variables $\ln p_*$, T, and q in the region R, but also for the external wind and the harmonic parts of these scalar variables in the region Q. The predicted results will be very smooth over the global surface for this two-way coupling method. Only some basic ideas of this two-way coupling method are mentioned, and how the external wind and harmonic parts of the region Q are computed based on the boundary values at Σ will not be discussed in this paper.

d. Some discussion on computation and boundary value problems

The semi-implicit time integration scheme is applied to the inner part equations of the model, and these inner part equations are solved by the double sine series, such as (4.24). During the computation of the spatial derivatives, if the lateral boundary values are homogeneous, for example, the computation of (5.1) and $\nabla^2\psi_i$ in (5.3), the double sine series are directly used; if the spatial derivatives of the harmonic function at the boundary need to be computed, such as (5.4), the solution of the harmonic function (CK92a) is used. As pointed out in section 1, the Tatsumi's (1986) modified Fourier series are useful in computation of the spatial derivatives, this method is also used in computing the spatial derivatives of the horizontal advection terms in this paper. The nonlinear advection terms are computed by the transform method (Orszag 1970; Eliassen et al. 1970), in which products are performed by transforming to the values at grid points, performing the product, and transforming back to wave space.

In the spectral method, the wavenumber truncation for avoiding the aliasing error was discussed by Canuto

et al. (1987, p. 84), which is sometimes referred to as the 3/2 rule. Chen (1993) found that using the 3/2 rule in the spectral model with the transform method is not necessary and the nonlinear computational instability induced by the aliasing terms is not present in the long-term integration. In our computations, it is also found that wavenumber truncation for avoiding the aliasing error is not necessary and the predicted results without the wavenumber truncation are better. The method without wavenumber truncation is used in this paper.

If a limited-area model is nested in a global model, there are two kinds of interaction at the boundary. One is the *boundary consistency problem*, which concerns whether the variables at the boundary predicted by two models are compatible (or continuous) with each other at the same time step $t = t_0 + \Delta t$. The boundary treatments studied by Benwell et al. (1971), Okamura (1975), and Davies (1976) are all aimed at solving this consistency problem, but the external wind lateral boundary method is very effective for this purpose.

The other kind of interaction at the boundary between two models is caused by horizontal transports of physical quantities, such as sensible heat and momentum fluxes. This problem may be referred to as *a boundary forcing problem.* This kind of interaction is a long-term effect, and it can be studied only by time integration of two models after the boundary consistency problem has been solved.

6. Some test results of the H-F spectral limited-area model with the external wind lateral boundary method

We now show some examples of the predicted results. The tests are performed with a view to check the validity of the H-F spectral method and one-way influence external wind lateral boundary values used in a limited-area model. In general, a new computational method or a new boundary procedure is often tested in a shallow-water model. However, the tests in this paper are demonstrated by the predicted results of the adiabatic dynamical part of the H-F spectral limited-area model. For this purpose, we choose examples for which diabatic effects are not important for the development of the major systems considered.

Because a comparison between the spectral method and finite difference method has been performed by Tatsumi (1986) and Juang and Kanamitsu (1994), we do not repeat it here.

a. Rapid cyclonic development along the east coast of North America

The first example is a rapid development of a cyclone near the east coast of North America. The topography of the model domain is shown in Fig. 4. In the vertical, 16 σ-levels at σ = 0.015, 0.045, 0.075, 0.105, 0.140, 0.200, 0.285, 0.390, 0.510, 0.630, 0.735, 0.825, 0.900, 0.950, 0.980, and 0.995 are used. The grid spacing is 180 km, and the total number of grid points is 61 $\times$ 51. A time step Δt of 30 min is used for the semi-implicit scheme.

The observed sea level pressure (SLP) and the geopotential height, temperature, and wind fields at the 500-hPa level at the initial time, 1200 UTC 4 January 1985, are shown in Figs. 5a and 5b; they are based on the analyses from the European Center for Medium-Range Weather Forecasts (ECMWF) at 2.5° $\times$ 2.5° resolution [TOGA Archive II from the National Center for Atmospheric Research (NCAR)]. The SLP for 0000 and 1200 UTC 5 and 0000 UTC 6 January 1985 and the geopotential height, temperature, and wind fields at the 500-hPa level for 1200 UTC 5 January 1985 are presented in Figs. 5c–f, respectively. The observed results show that a cyclone rapidly develops in the 24-h period from 0000 UTC 5 (Fig. 5c) to 0000 UTC 6 (Fig. 5e) January 1985 along the east coast of North America. In this 24-h period, the central pressure of the cyclone fell by about 27 hPa, which is greater than 1 bergeron [1 bergeron = 24 hPa day^{-1} ($\sin\phi/\sin 60°$), where ϕ, the latitude of the cyclone center, is about 50°]. This example was studied by Kuo and Low-Nam (1990), who found no significant difference in predicted intensity and location of this cyclone by using the NCAR–Penn State MM4 model with and without latent heat release. Thus, dry baroclinic instability is an extremely important factor for this explosive cyclogenesis case. This example is chosen with a view to assess the performance not only for the adiabatic dynamical part of the H-F spectral limited-area model but also for the external wind lateral boundary method.

In general, dry baroclinic instability is an important necessary condition for explosive oceanic cyclogenesis. If the dry baroclinic instability is strong enough, the baroclinic development alone can cause explosive cyclogenesis. In this case, the strong baroclinic instability is not only a necessary condition, but also a sufficient one. If the dry baroclinic development is not strong enough, other diabatic heating processes (latent heat release, sensible heat, and moisture fluxes at the lower boundary, and convective condensation feedback) are also necessary for the explosive development. In this latter case, the baroclinic instability together with the diabatic heating processes becomes the sufficient condition. The example chosen here belongs to the former case.

In the tests, the limited-area model is not nested in a global model. The boundary values are provided by the analyzed data instead of those from the prediction of a global model. The analyzed data are available only every 12 h, but the boundary values are required at each time step. The boundary values at each time step are linearly interpolated from analyzed data at 12-h intervals.

The external wind lateral boundary method discussed in section 5 is used in the tests, and there is no other boundary treatment in the model. As an example, the components of the external wind, U_E and V_E, at σ =

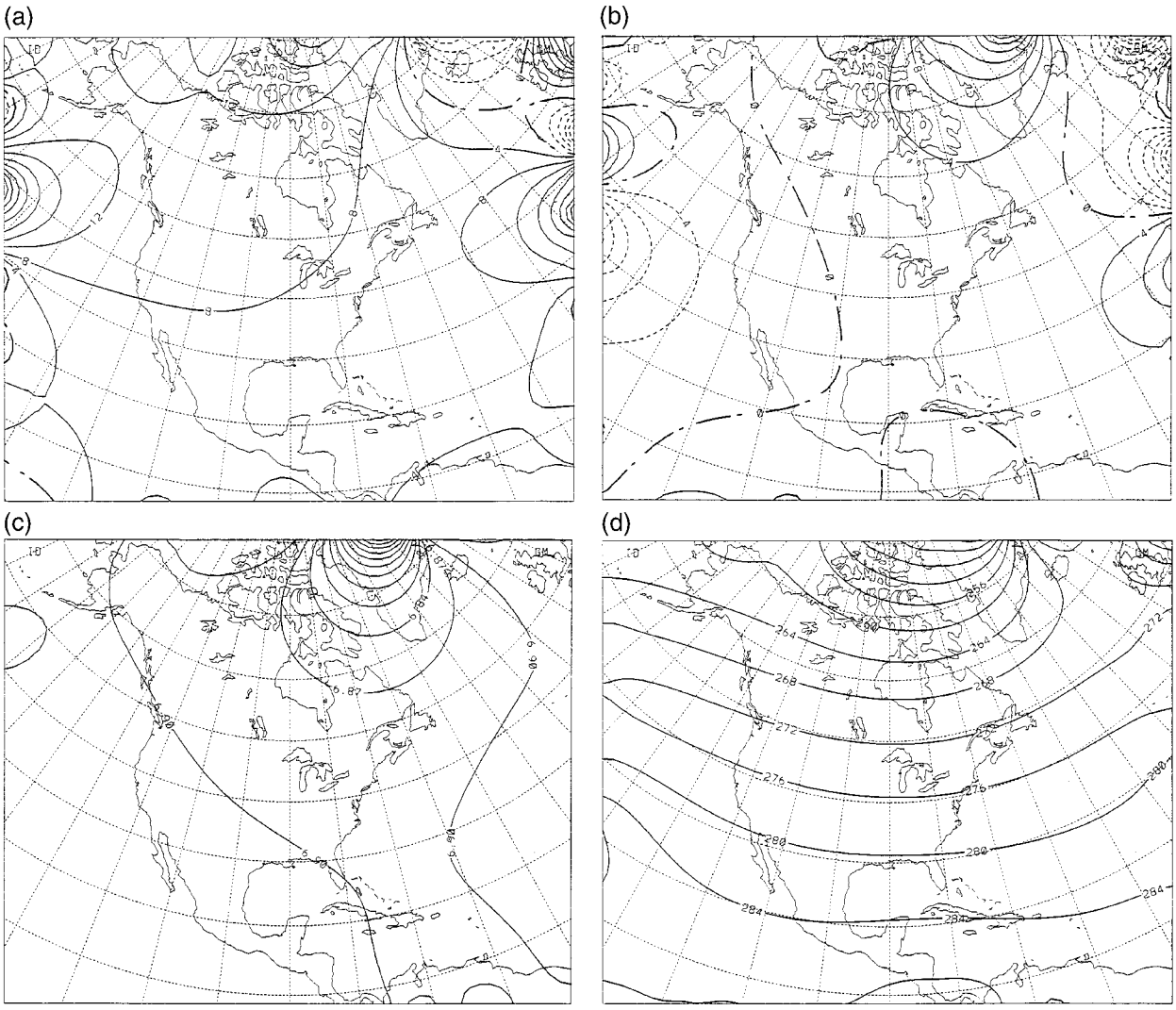

FIG. 6. An example of the lateral boundary conditions at 1200 UTC 4 January 1985: (a) the component of the external wind, U_E (in 4 m s^{-1} increments), at the level of $\sigma = 0.510$; (b) the same as (a) but for V_E; (c) the harmonic part of $\ln p_*$, i.e., $\ln p_{*h}$; and (d) the harmonic part of temperature, T_h (interval of 4 K), at the level $\sigma = 0.825$.

0.510 level for the initial time 1200 UTC January 4 1985 are shown in Figs. 6a and 6b, respectively. The boundary harmonic parts of the surface pressure, $\ln p_{*h}$, and the temperature, T_h, at $\sigma = 0.825$ level are determined by the simple method (5.5) except that the harmonic parts are derived from the analyzed data, and their values for the initial time are shown in Figs. 6c and 6d, respectively. Figures 6 show that they are all harmonic functions and attain their largest and smallest values at the boundary.

The 12-, 24-, and 36-h predictions of SLP are shown in Figs. 7a–c, respectively. It is seen from Fig. 7c that the predicted location of the developing cyclone is the same as the observed one in Fig. 5e. The predicted positions of all systems in Fig. 7c are very good. This is due to the fact that there is no systematic phase error in the spectral method. The rapid development of the cyclone is predicted very well by the adiabatic dynamical part of the model. The central pressure change predicted in 24 h from 0000 UTC 5 to 0000 UTC 6 January 1985 is about 25 hPa. The central pressure of the cyclone in Fig. 7c differs by only a small amount from that of the observations. The 12-, 24-, and 36-h predictions of the geopotential, temperature, and wind fields at the 500-hPa level are better than those of the SLP, but only the 24-h prediction is shown in Fig. 7d for comparison with the observations in Fig. 5f.

It is seen from Figs. 5a, 5c, and 5d that a cyclone moves into the region through the western boundary. In Fig. 5e, this cyclone is already within the region, and is followed by another cyclone coming through the same boundary. The 12-, 24-, and 36-h predicted results presented in Figs. 7a–c show that the cyclone gradually and smoothly moves into the region across the western

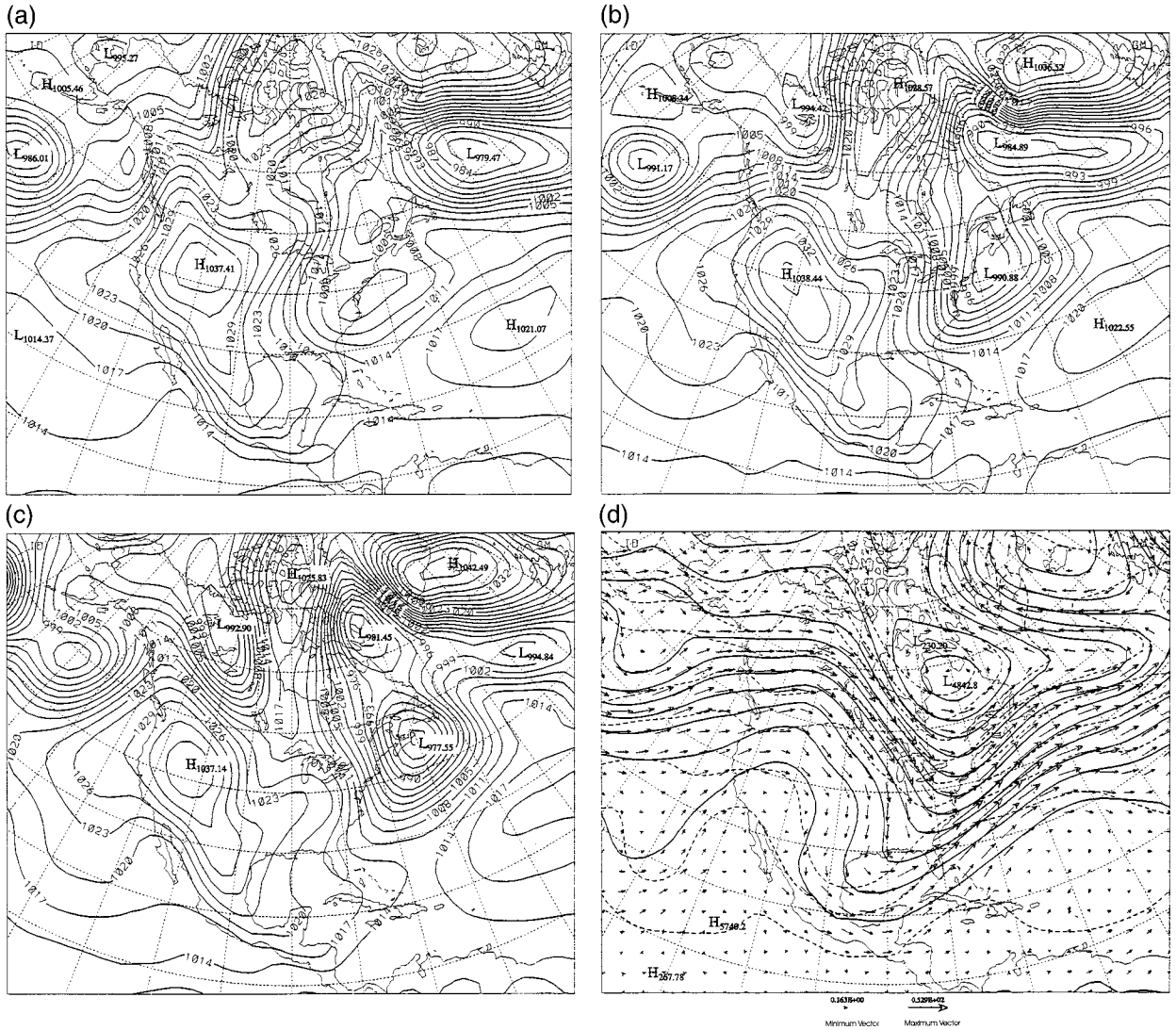

FIG. 7. The predicted results: (a) SLP at 0000 UTC 5 January 1985; (b) SLP at 1200 UTC 5 January 1985; (c) SLP at 0000 UTC 6 January 1985; and (d) the geopotential height, wind, and temperature at the 500-hPa level for same time as in (b).

boundary and is smoothly followed by the second cyclone (Fig. 7c). Thus, the boundary method is capable of transmitting motion systems smoothly into and out of the limited region. All the fields near the boundary shown in Figs. 7a–d are very smooth, and there is no discontinuity at the boundary.

Comparing Figs. 5e and 7c, some errors occur near Greenland. These errors are caused by two factors. One is due to the values being interpolated at 12-h intervals at the boundary where high mountains are cut off. The value of $\ln p_{*h}$ is very large at the boundary where high mountains are cut off, as shown in Fig. 6c over Greenland. If the boundary values are linearly interpolated from analyzed data at 12-h intervals, and the evolution of the true boundary values is produced by the nonlinear equations, some errors must be generated at the boundary. Thus, the errors of $\ln p_{*h}$ must be relatively large at this boundary. Tests show that the boundary errors expressed by harmonic functions do not produce any discontinuity at the boundary even though the errors are very large. This is an important advantage of the external wind lateral boundary method. However, the accuracy of the prediction is affected by the errors at the boundary. If the 12-h interpolation is removed by using the limited-area model nested in a global model or in a coarser limited-area model over a larger domain, the errors in prediction can be greatly reduced, which will be shown in the next example.

The second factor may be due to the strong cooling at the ice surface in winter over the Greenland Ice Sheet because of radiation and land–ice–atmosphere interactions in the PBL, which is not taken into account in the prediction of the adiabatic dynamical part of the limited-area model.

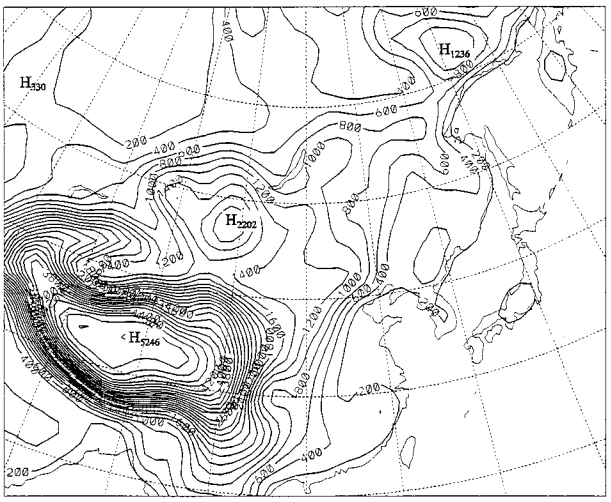

FIG. 8. The topography of the model domain over East Asia. Contour interval is 200 m.

b. *Lee cyclogenesis over East Asia and other phenomena related to the Tibetan Plateau*

Another example involves lee cyclogenesis over East Asia. Orographically forced cyclones, known as Alpine lee cyclones in Europe and Colorado and Alberta cyclones in North America, formed in the lee of the Rocky Mountains, have been studied by many authors (e.g., Palmen and Newton 1969; Buzzi and Speranza 1983). Although many major mountain barriers exist in East Asia, very few studies on lee cyclogenesis in this area have been done. Figure 8 shows the topography of the region defined for the limited-area model. Figures 4 and 8 are all computed from the U.S. Navy high resolution ($10' \times 10'$) dataset provided by NCAR. In the region shown by Fig. 8, the largest mountain is the huge Tibetan Plateau, whose maximum height is greater than 5000 m, and to the southwest of Lake Baikel, there are the Altai–Sayan Mountains, whose height is about 2200 m. The height and horizontal scale of the Altai–Sayan Mountains are comparable to those of the Alps. The topography of this region is the most complex in the world. The chosen example is to check whether or not the adiabatic dynamical part of the H-F spectral model can be used in this most orographically complicated region and to assess whether the external wind boundary values can be applied to the boundary where high mountains are cut off, as shown on the western boundary in Fig. 8.

c. *Lee cyclogenesis*

The observed SLP and the geopotential, temperature, and wind fields at the 500-hPa level for the initial time 1200 UTC 14 April 1988, based on the data from ECMWF, are shown in Figs. 9a,b, respectively. At 1200 UTC 14 April (Fig. 9a), a mature cyclone moves eastward to the north of Lake Baikal, which may be referred to as the parent cyclone according to Palmen and Newton (1969). A front trailing along the cyclone is oriented from northeast to southwest with a cold high behind. At the 500-hPa level (Fig. 9b), a major trough is located over the Urals with a diffluence of the height contours over the Altai–Sayan region. The SLP for 0000 and 1200 UTC 15 and 16 April 1988 and the geopotential, temperature, and wind fields at the 500-hPa level for 1200 UTC 15 and 16 April 1988 are presented in Figs. 9c–h, respectively. In Fig. 9c, a pressure ridge is formed on the windward side of Altai–Sayan when the front moving eastward is retarded by mountains. At the same time, the sea level pressure on the lee side of the mountains starts to fall and a low pressure trough appears over the Mongolian Plateau ahead of the front. Twelve hours later, as shown in Fig. 9d, a lee cyclone was formed with the central pressure about 996 hPa. At 0000 and 1200 UTC 6 April, as shown in Figs. 9e and 9f, this cyclone has grown to its mature state. However, the central pressure does not decrease, but increases and then stays unchanged at 999 hPa. The lee cyclone separates from the parent cyclone as the latter moves away from the limited region.

This example was simulated by Chen and Lazic (1990) with two experiments using a finite-difference limited-area model, of which the model description can be found in Mesinger et al. (1988). One experiment is performed with a ''step mountain'' (eta) coordinate (Mesinger and Janjic 1986) and the other with standard sigma coordinates. The horizontal resolution used for these experiments was $0.5^\circ \times 0.5^\circ$ with 16 levels in the vertical. It was found that the ETA experiment produced the cyclogenesis in a way similar to that in the analyses both at the surface and in the midtroposphere.

In our numerical simulation of this example, 16 σ levels in the vertical are the same as given in the last subsection. The grid length is 120 km, and the total number of grid points is 61×51. The time step Δt is 20 min for the semi-implicit scheme.

As pointed out in the above example, the accuracy of the prediction is affected by the errors at the boundary due to the linear interpolation from 12-h intervals, especially by the errors in $\ln p_{*_h}$ at the boundary where high mountains are cut off, as shown on the western side of Fig. 8. To avoid this error at the boundary, a coarser limited-area model over a larger domain is used to provide the boundary values to the fine-mesh limited-area model. The coarse-mesh model is the same spectral limited-area model with the same total grid points 61×51, but it is over a larger domain than Fig. 8 with the grid length of 240 km. The coarse-mesh model runs first for 48-h prediction with the lateral boundary condition derived from the linear interpolation of the analyzed values of 12-h intervals. Then the boundary values of the fine-mesh model are interpolated from the predicted values of the coarse-mesh model every 3 h. This boundary method is used in the simulation for the region shown in Fig. 8.

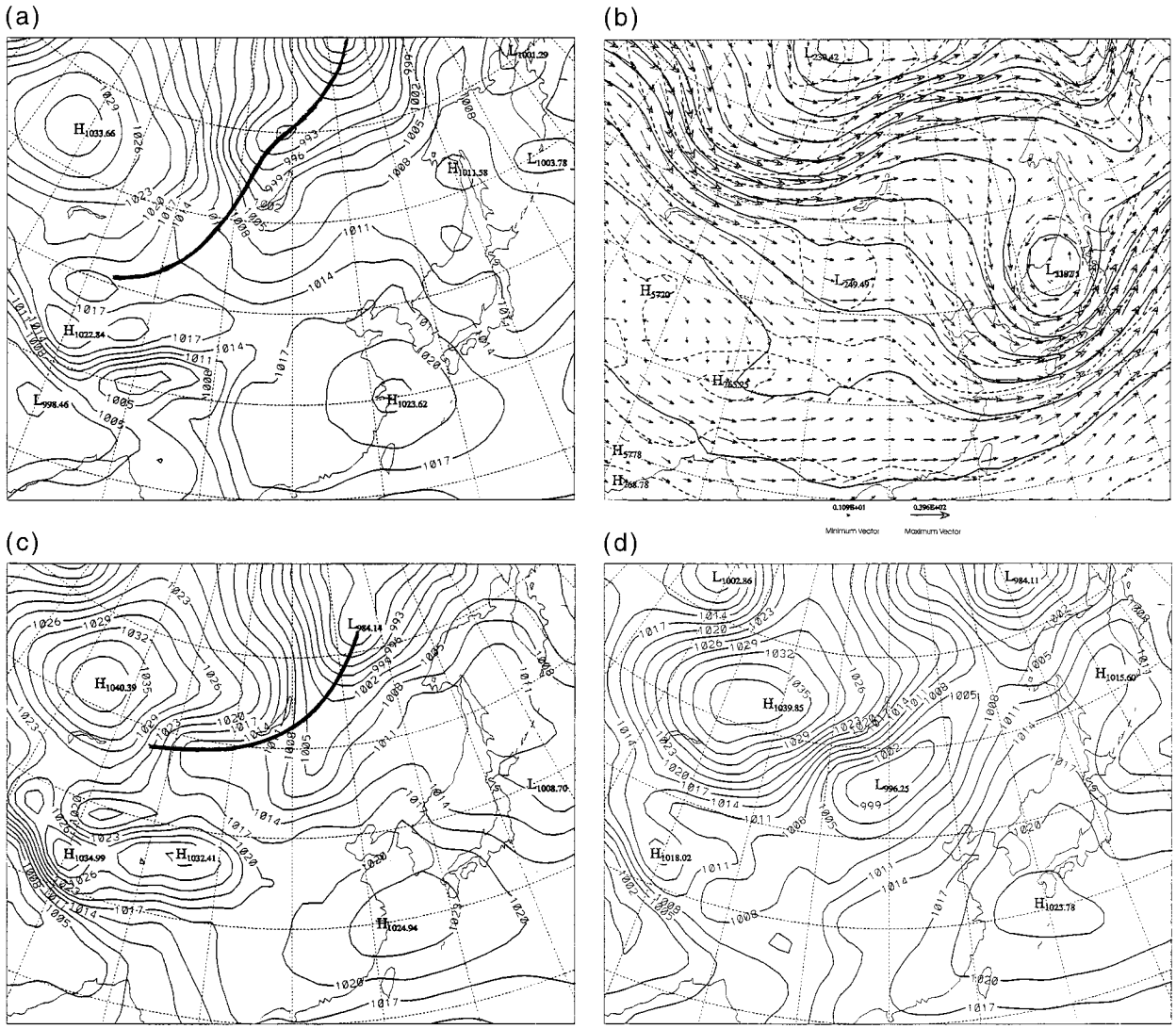

FIG. 9. Observed charts: (a) SLP at 1200 UTC 14 April 1988 (the heavy solid line denotes a front); (b) the geopotential height, wind, and temperature at the 500-hPa level for the same time as in (a); (c) SLP at 0000 UTC 15 April 1988; (d) SLP at 1200 UTC 15 April 1988; (e) SLP at 0000 UTC 16 April 1988; (f) SLP at 1200 UTC 16 April 1988; (g) the geopotential height, wind, and temperature at the 500-hPa level for same time as in (d); and (h) the geopotential height, wind, and temperature at the 500-hPa level for same time as in (f).

The predicted SLP for 12, 24, 36, and 48 h and predicted geopotential, temperature, and wind fields at 500-hPa level for 24 and 48 h from the initial time are shown in Figs. 10a–f, respectively. In Fig. 10a, a predicted pressure ridge is also formed on the windward side of Altai–Sayan and a low pressure trough appears over the Mongolian Plateau ahead of the front, which is the same as the observed situation in Fig. 9c. In the prediction for 12 h later shown in Fig. 10b, a lee cyclone is formed and its central pressure is 994 hPa, about 2 hPa lower than the observed. The predicted cyclone at 0000 and 1200 UTC 16 April shown in Figs. 10c,d develops to its mature stage. However, the predicted central pressure of the lee cyclone does not decrease but increases to 998 and 999 hPa, respectively. Its simulated maturation is the same as that analyzed in Figs. 9d and 9e. From the above, it is seen that the position, intensity, and maturation process of the predicted lee cyclone are very similar to those of the analyzed. Compared to the simulated results of Chen and Lazic (1990), a more accurate position, intensity, and maturation process of the surface lee cyclone are predicted by the H-F spectral model with less horizontal resolution and without the step-mountain coordinate.

d. Other phenomena

From 1200 UTC 15 (Fig. 9d) to 1200 UTC 16 (Fig. 9f) April 1988, the anticyclone behind the lee cyclone moves toward the southeast, and it causes cold air to affect the northeastern part of the Tibetan Plateau. It

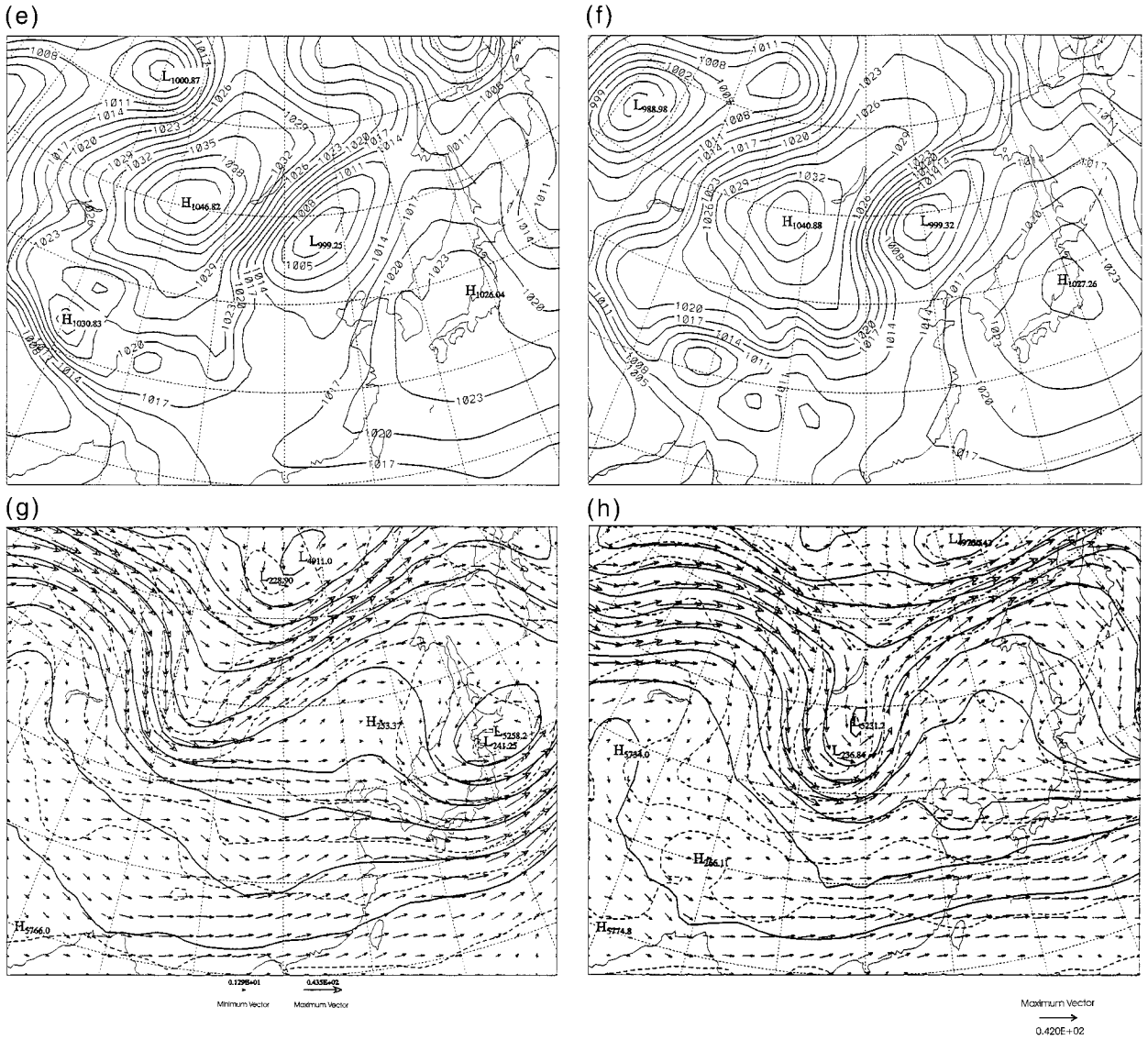

FIG. 9. (*Continued*)

can also be seen from the wind and temperature fields at 500-hPa level that cold-air advection appears in advance of the upper trough (Fig. 9g) and ultimately develops into a small midtropospheric cutoff low (Fig. 9h).

In the predictions for 1200 UTC 15 (Fig. 10b) and 16 (Fig. 10d), the anticyclone to the west of the lee cyclone also moves toward southeast. The positions of the high pressure in Figs. 9f and 10d are similar, but the predicted central pressure is higher than the observed. The predicted wind and temperature fields at the 500-hPa level also show that cold-air advection occurs in advance of the upper trough (Fig. 10e) and ultimately develops into a small midtropospheric cutoff low (Fig. 10f). Chen and Lazic (1990) found that the experiment with the standard sigma coordinate failed to simulate the upper cutoff low. It is seen from Fig. 10f that the upper cutoff low can also be simulated the H-F spectral model with the standard sigma coordinate. The cold air affecting the northeastern part of the Tibetan Plateau is predicted but not as strongly as that observed.

e. Phenomena over the Tibetan Plateau

Weather analysis over the Tibetan Plateau is a difficult and unsolved problem, and so is numerical weather prediction near this region. The synoptic analysis at sea level and at the 850- and 700-hPa levels over the Tibetan Plateau are all extrapolated from the upper troposphere. Weather systems in these analyses, including the analyzed data from ECMWF, are very difficult to identify. Both analysis methods and numerical weather prediction over this region should be improved.

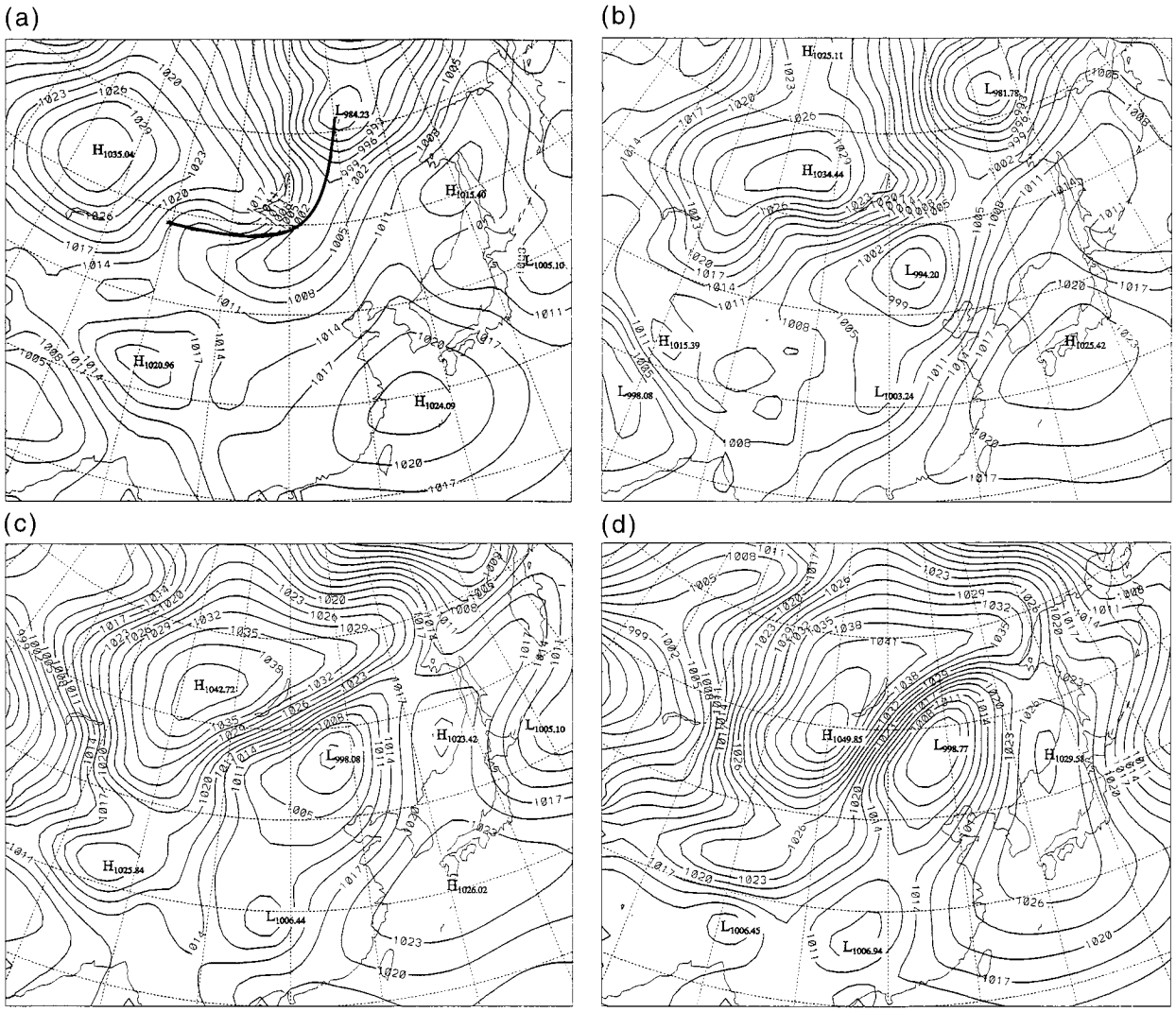

FIG. 10. The predicted results: (a) SLP at 0000 UTC 15 April 1988; (b) SLP at 1200 UTC 15 April 1988; (c) SLP at 0000 UTC 16 April 1988; (d) SLP at 1200 UTC 16 April 1988; (e) the geopotential height, wind, and temperature at the 500-hPa level for same time as in (b); and (f) the geopotential height, wind, and temperature at the 500-hPa level for same time as in (d).

In the SLP analysis from ECMWF shown in Figs. 9a, 9c, 9d, and 9e, there is a high pressure area over the western region of the Tibetan Plateau. The first step for modeling over the Tibetan Plateau is to test the model predictions against the analyses from ECMWF including the SLP. It is found that the spectral limited-area model with the external wind boundary values can smoothly run over this most orographically complicated region. The predicted results shown in Figs. 10a, 10b, and 10c also have the high pressure area over the western region of the Plateau.

Routine weather analysis method in the lower troposphere cannot identify weather systems moving across the Tibetan Plateau, but such weather systems do exist and often produce precipitation over Sichuan Basin and other downstream regions after they move out of the plateau. Comparing Figs. 9g and 10e, a trough in the lower troposphere moving to the east of the Tibetan Plateau is predicted by the H-F spectral model. This trough in the 24-h prediction is correct, but it is too strong in the 48-h prediction (Figs. 9h and 10f). Recently, an isobaric geopotential height in σ coordinates (Chen and Bromwich 1996) has been proposed. It can improve the performance of the H-F spectral limited-area model over the Tibetan Plateau and other mountainous regions, and this will be discussed elsewhere.

7. Conclusions

Based on the tests of the H-F spectral limited-area model with the external wind lateral boundary values discussed in the above sections, the following conclusions can be reached.

1) The harmonic-sine spectral method is very useful.

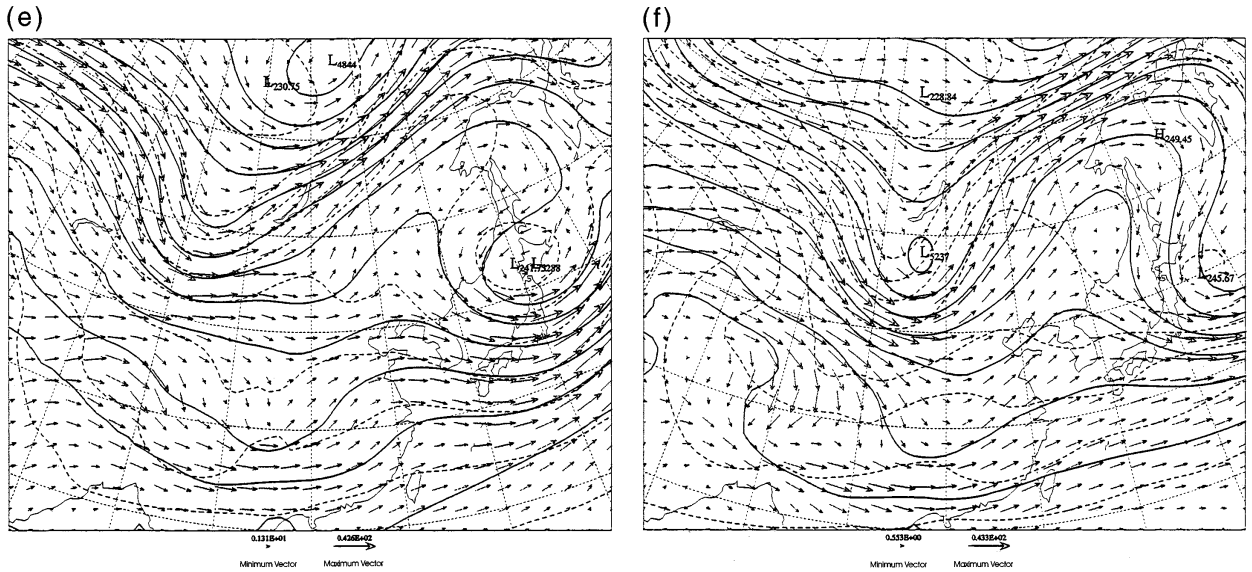

FIG. 10. (*Continued*)

In comparison with the modified double Fourier series used by Tatsumi (1986), the harmonic-sine spectral method has two advantages. (i) The semi-implicit scheme is quite efficient because the computation for the Laplacian operator and the derivation for the solutions of the Poisson and Helmholtz equations are made very simple by this spectral method. (ii) The lateral boundary value problem of a limited-area model can easily be solved by the external wind boundary method. These two advantages are similar to those of the spherical harmonic series used in global models.

2) The external wind lateral boundary method is proposed and examined for solving the lateral boundary problem of a limited-area model. The theoretical basis for this method is the basic property of the wind separation in a limited region. If a limited-area model is nested in a global model, the internal wind depends only on the vorticity and divergence inside the region and is predicted by the limited-area model, while the external wind depends only on the vorticity and divergence outside the limited region and it is predicted by the global model. The external wind in the limited region can be obtained by the natural method from the predicted wind of the global model. At each time step, the predicted total wind is the sum of the internal and external winds.

A similar method can also be used to solve the lateral boundary values of the scalar variables, such as the geopotential height, temperature, and surface pressure. The boundary values for a limited-area model can be given by the external wind and the harmonic parts of the above scalar variables. In this method, the boundary values are not given at the closed boundary line of the limited region, but always given by the harmonic functions defined in the whole limited domain. The derivatives of the harmonic function up to second order are continuous within the region up to the boundary. The harmonic functions added to the inner part represent the effect of the lateral boundary values on the prediction of the limited-area model. This procedure cannot cause any discontinuity of the variables near the boundary.

3) The prediction of a limited-area model at each time step can be computed by the sum of two parts: the prediction of the internal wind and inner part, and the prediction of the external wind and harmonic part. The prediction of the internal wind and inner part is derived from the inner part equations of the limited-area model. The boundary values of the inner parts are all homogeneous, and thus inner part equations can be solved easily by the double sine series. The semi-implicit scheme is quite easily and efficiently used for the inner part equations, the form of whose solutions is quite similar to that of the global spectral model except that the spherical harmonics are replaced by the double sine series. In addition, because the double sine series expansion can be calculated by FFT, its computation is faster and easier than that of the spherical harmonics in global models.

4) From the tests of the two cases of the one-way external wind lateral boundary method, it is shown that the predicted variables near the lateral boundary are very smooth without any other boundary treatment. The predicted motion systems can smoothly move in and out through the boundary and no wave reflection and small perturbations develop near the lateral boundary. The model can smoothly run over the complicated mountainous region shown in Fig. 8. The proposed boundary method can also be used at the boundary where high mountains are cut off, as shown in the western boundary of Fig. 8. Thus, by using the external wind boundary method, the difficulties of the lateral boundary values

associated with a limited-area model are greatly reduced.

5) The test of the rapid growth of a cyclone on the east coast of North America shows that the dynamical part of the H-F spectral limited-area model accurately predicts the rapid development caused by dry baroclinic instability. The location of predicted cyclone is the same as the observed, and the positions of other systems are also predicted very well. The central pressure change of the cyclone in the 24-h period from 0000 UTC 5 January to 6 January 1985 is about 25 hPa, which differs only slightly from the observations. The 12-, 24-, and 36-h prediction of the SLP and geopotential, temperature, and wind fields at 500-hPa level are very similar to those observed.

6) The test of a lee-cyclogensis case in East Asia shows that the predicted position and intensity of the cyclone are quite similar to those observed. The observed development of this lee cyclone indicates that a low pressure trough first appears over the Mongolian Plateau ahead of the front, and then the lee cyclone develops. However, the central pressure of the lee cyclone does not decrease but increases when it grows to its mature state. The predicted maturation processes are quite similar to those observed. Cold air associated with an anticyclone affecting the northeastern part of the Tibetan Plateau is also predicted by the model.

The H-F spectral limited-area model needs to be completed with a full package of physical parameterizations and to be further tested.

Acknowledgments. The authors would like to thank Dr. Ching-Yen Tsay for his helpful encouragement, support, and comments on this study. We would like also to thank the editor, Dr. Piotr Smolarkiewicz, and two anonymous reviewers for their valuable comments. This research was supported by Central Weather Bureau, Taipei, Taiwan, China, under Contracts CWB83-3M-01 and CWB84-3M-09 and by the NOAA Office of Global Programs via Grant NA36GP0314-01.

APPENDIX

The Vertical Finite-Difference Form of the Equations

The vertical distribution of variables is shown in Fig. 1: We define

$$\Delta\sigma_k = \sigma_{k+1/2} - \sigma_{k-1/2}. \tag{A.1}$$

The vertical advection of a variable X is approximated by

$$\left(\dot{\sigma}\frac{\partial X}{\partial \sigma}\right)_k \approx \frac{1}{2\Delta\sigma_k}[\dot{\sigma}_{k+1/2}(X_{k+1} - X_k) + \dot{\sigma}_{k-1/2}(X_k - X_{k-1})]. \tag{A.2}$$

a. The continuity equation

Using the boundary conditions

$$\dot{\sigma}\big|_{\sigma=0} = 0 \quad \text{and} \quad \dot{\sigma}\big|_{\sigma=1} = 0 \tag{A.3}$$

and (2.4), the local surface pressure tendency is expressed by

$$\frac{\partial \ln p_*}{\partial t} = -\int_0^1 (\delta + \mathbf{V}\cdot\nabla \ln p_*)\, d\sigma = -\int_0^1 \delta\, d\sigma - \int_0^1 \mathbf{V}\, d\sigma\cdot\nabla \ln p_* \tag{A.4}$$

and its vertical difference form is

$$\frac{\partial \ln p_*}{\partial t} = -\sum_{j=1}^{N} \delta_j\Delta\sigma_j - \sum_{j=1}^{N} \mathbf{V}_j\cdot\nabla \ln p_*\Delta\sigma_j. \tag{A.5}$$

Substituting (A.4) into (2.4) and integrating from 0 to σ, $\dot{\sigma}$ is given by

$$\dot{\sigma} = \sigma\left(\int_0^1 \delta\, d\sigma - \frac{1}{\sigma}\int_0^\sigma \delta\, d\sigma\right) + \sigma\left(\int_0^1 \mathbf{V}\cdot\nabla \ln p_*\, d\sigma - \frac{1}{\sigma}\int_0^\sigma \mathbf{V}\cdot\nabla \ln p_*\, d\sigma\right). \tag{A.6}$$

Both the sigma vertical velocity and local pressure tendency can be divided into their divergence part and surface pressure advection part, and their vertical difference forms are written as

$$\dot{\sigma}_{k+1/2} = \dot{\sigma}_{\text{div},k+1/2} + \dot{\sigma}_{\text{spa},k+1/2} \tag{A.7}$$

$$\dot{\sigma}_{\text{div},k+1/2} = \sigma_{k+1/2}\sum_{j=1}^{N} \delta_j\Delta\sigma_j - \sum_{j=1}^{k} \delta_j\Delta\sigma_j \tag{A.8}$$

$$\dot{\sigma}_{\text{spa},k+1/2} = \sigma_{k+1/2}\sum_{j=1}^{N} \mathbf{V}_j\cdot\nabla \ln p_*\Delta\sigma_j - \sum_{j=1}^{k} \mathbf{V}_j\cdot\nabla \ln p_*\Delta\sigma_j \tag{A.9}$$

$$\left(\frac{\partial \ln p_*}{\partial t}\right)_{\text{div}} = -\sum_{j=1}^{N} \delta_j\Delta\sigma_j \tag{A.10}$$

$$\left(\frac{\partial \ln p_*}{\partial t}\right)_{\text{spa}} = -\sum_{j=1}^{N} \mathbf{V}_j\cdot\nabla \ln p_*\Delta\sigma_j. \tag{A.11}$$

The pressure vertical velocity is written as

$$\frac{\omega}{p} = \frac{\dot{\sigma}}{\sigma} + \ln\dot{p}_* = \frac{\dot{\sigma}}{\sigma} + \frac{\partial \ln p_*}{\partial t} + \mathbf{V}\cdot\nabla \ln p_*. \tag{A.12}$$

Using (A.4) and (A.6), (A.12) is rewritten as

$$\frac{\omega}{p} = -\frac{1}{\sigma}\int_0^\sigma \delta\, d\sigma + \left(\mathbf{V}\cdot\nabla \ln p_* - \frac{1}{\sigma}\int_0^\sigma \mathbf{V}\cdot\nabla \ln p_*\, d\sigma\right), \tag{A.13}$$

and its vertical finite-difference form is

$$\left(\frac{\omega}{p}\right)_k = \mathbf{V}_k\cdot\nabla \ln p_* - \sum_{l=1}^{k} C_{kl}\mathbf{V}_l\cdot\nabla \ln p_* - \sum_{l=1}^{k} C_{kl}\delta_l, \tag{A.14}$$

where $\mathbf{C}$ is a lower-triangle matrix,

$$\mathbf{C} = \begin{bmatrix} \Delta\sigma_1/\sigma_1 & 0 & 0 & \cdots & 0 \\ \Delta\sigma_1/\sigma_2 & \Delta\sigma_2/\sigma_2 & 0 & \cdots & 0 \\ \Delta\sigma_1/\sigma_3 & \Delta\sigma_2/\sigma_3 & \Delta\sigma_3/\sigma_3 & \cdots & 0 \\ \cdot & \cdot & \cdot & \cdots & \cdot \\ \cdot & \cdot & \cdot & \cdots & 0 \\ \Delta\sigma_1/\sigma_N & \Delta\sigma_2/\sigma_N & \Delta\sigma_3/\sigma_N & \cdots & \Delta\sigma_N/\sigma_N \end{bmatrix}. \tag{A.15}$$

Using the vector form (2.25), the surface pressure advection term P_{adv} is expressed by

$$P_{\text{adv}} = -m^2\sum_{j=1}^{N}\left(U_j\frac{\partial \ln p_*}{\partial x} + V_j\frac{\partial \ln p_*}{\partial y}\right)\Delta\sigma_j - (m^2)'\mathbf{\Pi}\mathbf{D}. \tag{A.16}$$

Equation (A.14) is rewritten as

$$\left(\frac{\boldsymbol{\omega}}{p}\right) = m^2(\mathbf{I} - \mathbf{C})\left(\mathbf{U}\frac{\partial \ln p_*}{\partial x} + \mathbf{V}\frac{\partial \ln p_*}{\partial y}\right) - m^2\mathbf{C}\mathbf{D}, \tag{A.17}$$

where $\mathbf{I}$ is a unit matrix. The horizontal divergence part of $\boldsymbol{\omega}$ is expressed by

$$\left(\frac{\boldsymbol{\omega}}{p}\right)_{\text{div}} = -m^2\mathbf{C}\mathbf{D}, \tag{A.18}$$

and its surface pressure advection part is

$$\left(\frac{\boldsymbol{\omega}}{p}\right)_{\text{spa}} = m^2(\mathbf{I} - \mathbf{C})\left(\mathbf{U}\frac{\partial \ln p_*}{\partial x} + \mathbf{V}\frac{\partial \ln p_*}{\partial y}\right). \tag{A.19}$$

b. The hydrostatic equation

The integration of the hydrostatic equation (2.6) gives

$$\phi_k - \phi_{k+1} = -RT_{v,k+1/2}\ln\left(\frac{\sigma_k}{\sigma_{k+1}}\right), \qquad k < N, \tag{A.20}$$

and

$$\phi_N - \phi_* = -RT_{v,N}\ln\sigma_N, \tag{A.21}$$

where the mass-weighted mean temperature is

$$T_{v,k+1/2} = \frac{T_{v,k+1}\Delta\sigma_{k+1} + T_{v,k}\Delta\sigma_k}{\Delta\sigma_k + \Delta\sigma_{k+1}}, \tag{A.22}$$

and the same temperature at the surface and at N level are assumed; $\phi_* = gH_*$, where H_* is the height of the earth surface.

We define two parameters α_j and β_j as follows:

$$\alpha_j = -\frac{\Delta\sigma_j}{\Delta\sigma_j + \Delta\sigma_{j-1}}\ln\frac{\sigma_{j-1}}{\sigma_j}, \qquad N \ge j \ge 2$$

$$\beta_j = \begin{cases} -\ln\sigma_j, & j = N \\ -\dfrac{\Delta\sigma_j}{\Delta\sigma_{j+1} + \Delta\sigma_j}\ln\dfrac{\sigma_j}{\sigma_{j+1}}, & j < N \end{cases}. \tag{A.23}$$

From (A.21) we have

$$\phi_N = \phi_* + R\beta_N T_{v,N} \tag{A.24}$$

and for $k = N - 1$,

$$\phi_{N-1} = \phi_N + R(\beta_{N-1}T_{v,N-1} + \alpha_N T_{v,N}) = \phi_* + R\beta_{N-1}T_{v,N-1} + R(\beta_N + \alpha_N)T_{v,N}. \tag{A.25}$$

For $k = N - 2$, we have

$$\phi_{N-2} = \phi_* + R\beta_{N-2}T_{v,N-2} + R(\beta_{N-1} + \alpha_{N-1})T_{v,N-1} + R(\beta_N + \alpha_N)T_{v,N}. \tag{A.26}$$

On generalizing, we get

$$\phi_k = \phi_* + R\beta T_{v,k} + R(\beta_{k+1} + \alpha_{k+1})T_{v,k+1} + \ldots + R(\beta_{N-1} + \alpha_{N-1})T_{v,N-1} + R(\beta_N + \alpha_N)T_{v,N}. \tag{A.27}$$

Consider a finite-difference form of the hydrostatic equation,

$$\phi_k = \phi_* + R\sum_{l=k}^{n} B_{kl}T_{vl}, \tag{A.28}$$

where B_{kl} are elements of a matrix $\mathbf{B}$ expressed by

$$\mathbf{B} = \begin{bmatrix} \beta_1 & \beta_2 + \alpha_2 & \beta_3 + \alpha_3 & \cdots & \beta_N + \alpha_N \\ 0 & \beta_2 & \beta_3 + \alpha_3 & \cdots & \beta_N + \alpha_N \\ 0 & 0 & \beta_3 & \cdots & \beta_N + \alpha_N \\ \cdot & \cdot & \cdot & \cdots & \cdot \\ \cdot & \cdot & \cdot & \cdots & \beta_N + \alpha_N \\ 0 & 0 & 0 & \cdots & \beta_N \end{bmatrix}. \tag{A.29}$$

c. The thermodynamic equation

Utilizing (A.12), (2.3) can be written as

$$\frac{\partial T}{\partial t} = -m^2\left(\frac{u}{m}\frac{\partial T'}{\partial x} + \frac{v}{m}\frac{\partial T'}{\partial y}\right) - \sigma^{\kappa}\dot{\sigma}\frac{\partial T\sigma^{-\kappa}}{\partial \sigma} + \kappa T \ln\dot{p}_* + P_T + K_T, \quad \text{(A.30)}$$

where $\kappa = R/C_p$. Based on the separation of the vertical velocity, (A.30) can be rewritten in the form

$$\frac{\partial T'}{\partial t} = -\sigma^{\kappa}\frac{\partial T_0\sigma^{-\kappa}}{\partial \sigma}\dot{\sigma}_{\text{div}} + \kappa T_0\left(\frac{\partial \ln p_*}{\partial t}\right)_{\text{div}} + T_{\text{adv}} + P_T + K_T, \quad \text{(A.31)}$$

where

$$T_{\text{adv}} = -m^2\left(\frac{u}{m}\frac{\partial T'}{\partial x} + \frac{v}{m}\frac{\partial T'}{\partial y}\right) - \sigma^{\kappa}\frac{\partial T'\sigma^{-\kappa}}{\partial \sigma}\dot{\sigma}_{\text{div}} + \kappa T'\left(\frac{\partial \ln p_*}{\partial t}\right)_{\text{div}} - \sigma^{\kappa}\frac{\partial T\sigma^{-\kappa}}{\partial \sigma}\dot{\sigma}_{\text{spa}} + \kappa T\left(\frac{\partial \ln p_*}{\partial t}\right)_{\text{spa}} + \kappa T m^2\left(\frac{u}{m}\frac{\partial \ln p_*}{\partial x} + \frac{v}{m}\frac{\partial \ln p_*}{\partial y}\right). \quad \text{(A.32)}$$

The vertical difference form of (A.31) is

$$\frac{\partial T'_k}{\partial t} = T'_{\text{adv},k} - m^2\sum_{l=1}^{N} F_{k,l}D_l + P_{T,k} + K_{T,k}, \quad \text{(A.33)}$$

where the elements of matrix $\mathbf{F}$ are defined as

$$F_{k,l} = \frac{\sigma_k^{\kappa}}{2\Delta\sigma_k}[(T_{0,k+1}\sigma_{k+1}^{-\kappa} - T_{0,k}\sigma_k^{-\kappa})(\sigma_{k+1/2}\Delta\sigma_l - \epsilon_1) + (T_{0,k}\sigma_k^{-\kappa} - T_{0,k-1}\sigma_{k-1}^{-\kappa})(\sigma_{k-1/2}\Delta\sigma_l - \epsilon_2)] + \kappa T_{0,k}\Delta\sigma_l \quad \text{(A.34)}$$

and

$$\epsilon_1 = \begin{cases} 0, & \text{if } l > k, \\ \Delta\sigma_l, & \text{if } l \le k, \end{cases}$$

$$\epsilon_2 = \begin{cases} 0, & \text{if } l > k-1, \\ \Delta\sigma_l, & \text{if } l \le k-1. \end{cases} \quad \text{(A.35)}$$

The temperature advection can be separated into three parts as

$$T'_{\text{adv},k} = T_{\text{hor},k} + T_{\text{ver},k} + T_{\text{spa},k}, \quad \text{(A.36)}$$

where

$$T_{\text{hor},k} = -m^2\left(U_k\frac{\partial T'_k}{\partial x} + V_k\frac{\partial T'_k}{\partial y}\right) \quad \text{(A.37)}$$

is the temperature variation due to the horizontal advection and

$$T_{\text{ver},k} = -\frac{\sigma_k^{\kappa}}{2\Delta\sigma_k}[\dot{\sigma}_{\text{div},k+1/2}(T'_{k+1}\sigma_{k+1}^{-\kappa} - T'_k\sigma_k^{-\kappa}) + \dot{\sigma}_{\text{div},k-1/2}(T'_k\sigma_k^{-\kappa} - T'_{k-1}\sigma_{k-1}^{-\kappa})] + \kappa T'_k\left(\frac{\partial \ln p_*}{\partial t}\right)_{\text{div}} \quad \text{(A.38)}$$

is caused by the temperature deviation due to divergence part of the vertical motion. Here $(\partial \ln p_*/\partial t)_{\text{div}}$ and $\dot{\sigma}_{\text{div},k+1/2}$ are shown by (A.10) and (A.8), respectively. The temperature variation due to the surface pressure advection, $T_{\text{spa},k}$, is expressed by

$$T_{\text{spa},k} = -\frac{\sigma_k^{\kappa}}{2\Delta\sigma_k}[\dot{\sigma}_{\text{spa},k+1/2}(T_{k+1}\sigma_{k+1}^{-\kappa} - T_k\sigma_k^{-\kappa}) + \dot{\sigma}_{\text{spa},k-1/2}(T_k\sigma_k^{-\kappa} - T_{k-1}\sigma_{k-1}^{-\kappa})] + \kappa T\left[\left(\frac{\partial \ln p_*}{\partial t}\right)_{\text{spa}} + m^2\left(U_k\frac{\partial \ln p_*}{\partial x} + V_k\frac{\partial \ln p_*}{\partial y}\right)\right], \quad \text{(A.39)}$$

where $(\partial \ln p_*/\partial t)_{\text{spa}}$ and $\dot{\sigma}_{\text{spa},k+1/2}$ are shown by (A.11) and (A.9), respectively.

d. The equations of vorticity, divergence, and mixing ratio

The vertical difference form of vorticity equation (2.14) is

$$\frac{\partial \Omega_k}{\partial t} = -f_0 D_k + \Omega_{\text{adv},k} + K_{\zeta,k}, \quad \text{(A.40)}$$

where

$$\Omega_{\text{adv},k} = -\left[U_k\frac{\partial}{\partial x}(f' + m^2\Omega_k) + V_k\frac{\partial}{\partial y}(f' + m^2\Omega_k)\right] - (f' + m^2\Omega_k)D_k + \left(\frac{\partial F_{v,k}}{\partial x} - \frac{\partial F_{u,k}}{\partial y}\right) \quad \text{(A.41)}$$

$$F_{u,k} = -\frac{1}{2\Delta\sigma_k}[\dot{\sigma}_{k+1/2}(U_{k+1} - U_k) + \dot{\sigma}_{k-1/2}(U_k - U_{k-1})] - RT'_{v,k}\frac{\partial \ln p_*}{\partial x} + \left(\frac{P_U}{m}\right)_k$$

$$F_{v,k} = -\frac{1}{2\Delta\sigma_k}[\dot{\sigma}_{k+1/2}V_{k+1} - V_k) + \dot{\sigma}_{k-1/2}(V_k - V_{k-1})] - RT'_{v,k}\frac{\partial \ln p_*}{\partial y} + \left(\frac{P_V}{m}\right)_k, \quad \text{(A.42)}$$

and that of the divergence equation (2.15) is

$$\frac{\partial D_k}{\partial t} = f_0\Omega_k - \nabla^2(\phi_k + RT_{0k}\ln P_*) + D_{\text{adv},k} - \nabla^2 E_k + K_{\delta,\mathbf{k}} \quad \text{(A.43)}$$

$$D_{\text{adv},k} = V_k\frac{\partial(f' + m^2\Omega_k)}{\partial x} - U_k\frac{\partial(f' + m^2\Omega_k)}{\partial y} + (f + m^2\Omega_k)\Omega_k + \frac{\partial F_{u,k}}{\partial x} + \frac{\partial F_{v,k}}{\partial y} \quad \text{(A.44)}$$

$$E_k = \frac{m^2}{2}(U_k^2 + V_k^2).$$

The vertical difference of the equation of the mixing ratio is

$$\frac{\partial q_k}{\partial t} = Q_{\text{adv},k} + P_{q,k} + K_{q,k}, \quad \text{(A.45)}$$

where

$$Q_{\text{adv},k} = -m^2\left(U\frac{\partial q_k}{\partial x} + V\frac{\partial q_k}{\partial y}\right) - \frac{1}{2\sigma_k}[\dot\sigma_{k+1/2}(q_{k+1} - q_k) + \dot\sigma_{k-1/2}(q_k - q_{k-1})]. \quad \text{(A.46)}$$

REFERENCES

Baede, A. P. M., M. Jarraud, and U. Cubasch, 1979: Adiabatic formulation and organization of ECMWF spectral model. ECMWF Tech. Rep. 15, 40 pp.

Benwell, G. R. R., A. J. Gadd, J. F. Keers, M. S. Timpson, and P. W. White, 1971: The Bushby–Timpson 10-level model on a fine mesh. Meteor. Office Scientific Paper 32.

Bourke, W., 1974: A multi-level spectral model. Part I: Formulation and hemispheric integrations. *Mon. Wea. Rev.*, **102,** 687–701.

Browning, G., and H.-O. Kreiss, 1986: Scaling and computation of smooth atmospheric motions. *Tellus,* **38A,** 295–313.

Buzzi, A., and A. Speranza, 1983: Cyclogenesis in the lee of Alps. *Mesoscale Meteorology—Theories, Observation and Models,* K. Lilly and T. Gal-Chen, Eds., Vol. 1, NATO ASI Series, Reidel, 52–107.

Canuto, C., M. Y. Hussaini, A. Quarteroni, and T. A. Zang, 1987: *Spectral Methods in Fluid Dynamics.* Springer-Verlag, 557 pp.

Charney, J. G., 1962: Integration of the primitive and balance equation. *Proc. Int. Symp. Numerical Weather Prediction,* Tokyo, Japan, Meteor. Soc. of Japan, 130–152.

Chen, Q.-S., and Y.-H. Kuo, 1992a: A harmonic-sine series expansion and its application to the partitioning and reconstruction problem in a limited area. *Mon. Wea. Rev.*, **120,** 91–112.

——, and ——, 1992b: A consistency condition for the wind field reconstruction in a limited area and a harmonic-cosine series expansion. *Mon. Wea. Rev.*, **120,** 2653–2670.

——, and D. H. Bromwich, 1996: An isobaric geopotential height and its application to synoptic analysis and to a generalized ω-equation in σ-coordinates. *15th Conf. on Weather Analysis and Forecasting,* Norfolk, VA, Amer. Meteor. Soc., 409–412.

——, Y.-H. Kuo, and D. H. Bromwich, 1996: A balanced ageostrophic initialization with an external wind lateral boundary value for limited-area models. *J. Meteor. Soc. Japan,* **74,** 325–342.

Chen, S.-J., and L. Lazic, 1990: Numerical case study of the Altai-Sayan lee cyclogenesis over east Asia. *Meteor. Atmos. Phys.*, **42,** 221–229.

Chen, X.-S., 1993: The aliased and the dealiased spectral models of the shallow-water equations. *Mon. Wea. Rev.*, **121,** 834–852.

Davies, H. C., 1976: A lateral boundary formulation for multi-level prediction models. *Quart. J. Roy. Meteor. Soc.*, **102,** 405–418.

Eliassen, E., B. Machenauer, and E. Rasmussen, 1970: On the numerical method for integration of the hydrodynamic equations with a spectral representation of the horizontal fields. Inst. of Theoretical Meteorology, University of Copenhagen Rep. 2, 35 pp.

Fulton, S. R., and W. H. Schubert, 1987a: Chebyshev spectral methods for limited-area models. Part I: Model problem analysis. *Mon. Wea. Rev.*, **115,** 1940–1953.

——, and ——, 1987b: Chebyshev spectral methods for limited-area models. Part II: Shallow water model. *Mon. Wea. Rev.*, **115,** 1954–1965.

Hack, J. J., and W. H. Schubert, 1981: Lateral boundary conditions for tropical cyclone models. *Mon. Wea. Rev.*, **109,** 1404–1420.

Haugen, J. E., and B. Machenhauer, 1993: A spectral limited-area model formulation with time-dependent boundary conditions applied to the shallow-water equations. *Mon. Wea. Rev.*, **121,** 2618–2630.

Hoskins, B. J., and A. J. Simmons, 1975: A multi-layer spectral model and the semi-implicit method. *Quart. J. Roy. Meteor. Soc.*, **101,** 637–655.

Juang, H.-M. H., and M. Kanamitsu, 1994: The NMC nested regional spectral model. *Mon. Wea. Rev.*, **122,** 3–33.

Kesel, P. G., and F. J. Winninghoff, 1972: The Fleet Numerical Weather Centre operational primitive equation model. *Mon. Wea. Rev.*, **100,** 300–373.

Kuo, H.-C., and R. T. Williams, 1992: Boundary effects in regional spectral methods. *Mon. Wea. Rev.*, **120,** 2986–2992.

Kuo, Y.-H., and S. Low-Nam, 1990: Prediction of nine explosive cyclones over the western Atlantic Ocean with a regional model. *Mon. Wea. Rev.*, **118,** 3–25.

Mesinger, F., and Z. Janjic, 1986: Numerical technique for representation of mountains. *Observation, Theory and Modelling of Orographic Effects,* Vol. 2, ECMWF, 29–80.

——, ——, S. Nickovic, D. Gavrilov, and D. G. Deaven, 1988: The step mountain coordinate: Model description and performance for cases of Alpine lee cyclogenesis and for a case of an Appalachian redevelopment. *Mon. Wea. Rev.*, **116,** 1493–1518.

Okamura, Y., 1975: Computational design of a limited-area prediction model. *J. Meteor. Soc. Japan,* **53,** 175–188.

Oliger, J., and A. Sundstrom, 1978: Theoretical and practical aspects of some initial-boundary value problems in fluid dynamics. *SIAM J. Appl. Math.*, **35,** 419–446.

Orszag, S. A., 1970: Transform method for calculation of vector coupled sum: Application to the spectral form of the vorticity equation. *J. Atmos. Sci.*, **27,** 890–895.

Palmen, E., and C. W. Newton, 1969: *Atmospheric Circulation Systems,* Academic Press, 419 pp.

Perkey, D. J., and C. W. Kreitzberg, 1976: A time-dependent lateral boundary scheme for limited-area primitive equation models. *Mon. Wea. Rev.*, **104,** 744–755.

Tatsumi, Y., 1986: A spectral limited area model with time-dependent lateral boundary conditions and its application to a multi-level primitive equation model. *J. Meteor. Soc. Japan,* **64,** 637–663.